BRNO UNIVERSITY OF TECHNOLOGY
VYSOKÉ UČENÍ TECHNICKÉ V BRNĚ

FACULTY OF MECHANICAL ENGINEERING
FAKULTA STROJNÍHO INŽENÝRSTVÍ

INSTITUTE OF PHYSICAL ENGINEERING
ÚSTAV FYZIKÁLNÍHO INŽENÝRSTVÍ

BIOSENSORS BASED ON FUNCTIONALIZED GRAPHENE
BIOSENZORY NA BÁZI FUNKCIONALIZOVANÉHO GRAFENU

MASTER'S THESIS
DIPLOMOVÁ PRÁCE

AUTHOR
AUTOR PRÁCE
Bc. Lucie Pavlásková

SUPERVISOR
VEDOUCÍ PRÁCE
doc. Ing. Miroslav Bartošík, Ph.D.

BRNO 2021

BRNO UNIVERSITY OF TECHNOLOGY
FACULTY OF MECHANICAL ENGINEERING

Assignment Master's Thesis

Institut:	Institute of Physical Engineering
Student:	**Bc. Lucie Pavlásková**
Degree programm:	Physical Engineering and Nanotechnology
Branch:	no specialisation
Supervisor:	**doc. Ing. Miroslav Bartošík, Ph.D.**
Academic year:	2020/21

As provided for by the Act No. 111/98 Coll. on higher education institutions and the BUT Study and Examination Regulations, the director of the Institute hereby assigns the following topic of Master's Thesis:

Biosensors based on functionalized graphene

Brief Description:

Thanks to its unique properties, especially: high mobility of charge carriers, compatibility with biological substances and changes in electrical properties caused by the influence of individual adsorbed biochemical molecules, graphene is an almost ideal material for use in biosensors . Its main disadvantage in this area is the fact that graphene reacts to any adsorbed molecule indiscriminately through changes in resistance and thus does not show in itself a sufficient selectivity in the detection of a specific biochemical compound. The aim of this work is to overcome this disadvantage through the appropriate functionalization of graphene so that the sensor based on functionalized graphene reacts selectively only to the selected biochemical substance .

Master's Thesis goals:

1. Literature retrieval of the mentioned issue with emphasis on suitable initial functionalization of graphene and detected biochemical compound.
2. Graphene functionalization and verification of functionalization efficiency (Raman spectroscopy, XPS, transport measurements).
3. Design and manufacture of a suitable graphene sensor based on functionalized graphene.
4. Measurement of the transport response of a graphene sensor to a suitable biochemical substance.
5. Analysis of results with regard to the effectiveness of functionalization, sensor sensitivity and especially its selectivity.

Recommended bibliography:

SCHEDIN, F., A. K. GEIM, S. V. MOROZOV, E. W. HILL, P. BLAKE, M. I. KATSNELSON a K. S. NOVOSELOV. Detection of individual gas molecules adsorbed on graphene. Nature Materials. 2007, 6(9), 652-655. DOI: 10.1038/nmat1967.

SHAO, Y., J. WANG, H. WU, J. LIU, I. A. AKSAY, Y. LIN. Graphene Based Electrochemical Sensors and Biosensors: A Review. Electroanalysis. 2010, 22(10), 1027-1036. DOI: 10.1002/elan.200900571.

NAG, A., A. MITRA, S. C. MUKHOPADHYAY. Graphene and its sensor-based applications: A review. Sensors and Actuators A: Physical. 2018, 270, 177-194. DOI: 10.1016/j.sna.2017.12.028.

KWAK, Y. H., D. S. CHOI, Y. N. KIM, H. KIM, D. H. YOON, S. S. AHN, J. W. YANG, W. S. YANG, S. SEO. Flexible glucose sensor using CVD-grown graphene-based field effect transistor. Biosensors and Bioelectronics. 2012, 37(1), 82-87. DOI: 10.1016/j.bios.2012.04.042.

SHAN, C., H. YANG, J. SONG, D. HAN, A. IVASKA, L. NIU. Direct Electrochemistry of Glucose Oxidase and Biosensing for Glucose Based on Graphene. Analytical Chemistry. 2009, 81(6), 2378-2382. DOI: 10.1021/ac802193c.

ZHU, Zanzan. An Overview of Carbon Nanotubes and Graphene for Biosensing Applications. Nano-Micro Letters. 2017, 9(3), 1-24. DOI: 10.1007/s40820-017-0128-6.

Abstract

In this work, a graphene field-effect transistor (GFET) was demonstrated as a sensing platform for glucose detection. The linker molecule pyrenebutanoic acid succinimidyl ester (PSE) and enzyme glucose oxidase (GOx) were successfully employed to functionalize the graphene channel in FET. The GOx enzyme was immobilized on the channel for glucose detection as it induces a selective catalytic glucose reaction. The functionalization process was characterized by Raman spectroscopy and Atomic force microscopy (AFM). The fabricated graphene-based biosensors enabled the electrical detection of glucose in two different setups. By the Dirac point shift in dependency of resistance on continual change of gate voltage and by the sample resistance response at constant gate voltage. This study indicates that graphene holds great promise for the development of nanoelectronic biosensors including glucose level monitoring applications.

Abstrakt

V této práci byl demonstrován grafenový polem řízený transistor (GFET) jako platforma pro detekci glukózy. Sukcinimidyl ester pyrenbutanové kyseliny (PSE) sloužící jako nosič a enzym glukóza oxidáza (GOx), byly úspěšně použity k funkcionalizaci grafenového kanálu v FE transitoru. Enzym GOx byl imobilizován na grafenovém kanálu pro glukózovou detekci, jelikož indukuje selektivní katalytickou reakci glukózy. Proces funkcionalizace byl charakterizován pomocí Ramanovy spektroskopie a Atomární silové mikroskopie (AFM). Vyrobený biosenzor na bázi grafenu umožnil elektrickou detekci glukózy ve dvou různých zapojeních. Prostřednictvím posunu Diracova bodu v závislosti odporu na spojité změně hradlového napětí a prostřednictvím jednoduché odporové odezvy při konstantním napětí na hradle. Tato studie naznačuje, že grafen je slibným materiálem pro vývoj nanoelektronických biosenzorů včetně aplikací pro monitorování hladiny glukózy.

Keywords

Biosensor, Functionalized graphene, Field-effect transistor, Glucose, Glucose oxidase

Klíčová slova

Biosenzor, Funkcionalizovaný grafen, Polem řízený tranzistor, Glukóza, Glukóza-oxidáza

PAVLÁSKOVÁ, L. *Biosenzory na bázi funkcionalizovaného grafenu.* Brno University of Technology, Fakulta strojního inženýrství, 2021. 63 s. Vedoucí doc. Ing. Miroslav Bartošík, Ph.D.

I declare that I have written the Master's Thesis titled "Biosensors based on functionalized graphene" independently, under the guidance of the advisor and using exclusively the technical references and other sources of information cited in the thesis and listed in the comprehensive bibliography at the end of the thesis.

Bc. Lucie Pavlásková

I would first like to thank my supervisor, doc. Ing. Miroslav Bartošík, Ph.D, for his valuable, professional guidance, latitude and the trust with which he accompanied me during the Master's and Bachelor's studies.
I would like to acknowledge Jakub Piastek and Vojtěch Švarc for their time, as they provided me with friendly technical support and assistance.
My thanks also go to my classmates, Petr, Ondřej, Peter, Ondrej and Jan, who have always been willing to help me, and together with my friends Radim and Marek, they formed the core of my entire university studies.
I would like to thank everyone from the Institute of Physical Engineering for the opportunity to be part of the IPE family.
I cannot thank enough my parents and my partner Jakub for their care and especially their patience, and support in difficult times.

Bc. Lucie Pavlásková

Contents

Introduction

Discussions regarding biological sensors have dominated research in recent years. This work focuses on the revolutionary two-dimensional graphene which is employed in the form of a sensing electrode channel for improving an analytical performance of a glucose biosensor. Thanks to its remarkable properties characterized by high electrical mobility, ambipolar effect, high electron transfer rate, as well as large specific surface area, and biocompatibility, graphene meets the requirements for application in an ideal biosensing system. The large specific surface area predetermines that graphene is highly responsive to changes on its surface.

In electrochemical biosensors, the detection is performed through a transducer element which transforms the changes on to an electrical signal. Such changes are caused by interactions between biomolecules that produce or consume electrons. In combination with high electrical mobility, graphene has a significant potential to be employed for direct charge carrier transfer between the biomolecules and electrode. However, biomolecules capable of specific and selective reaction with other biomolecules, bioreceptor molecules, must be immobilized on the surface of graphene. This is achieved by the functionalization of graphene which provides the best way to achieve a highly sensitive and selective response on relevant biochemical substances.

Over the last decades, rapid technological and economic developments affected personal lifestyles and have led to a significant increase in welfare diseases. Diabetes, characterized by an increased blood glucose level, is one of the most common. Historically, glucose monitoring is crucial both in the diagnosis of diabetes and in the overall development of biosensors. Therefore, it is not surprising that glucose-sensing devices dominate the global biosensor market and real-time sensing. Nevertheless, it is not only healthcare that is fascinated by glucose detection, but there is both strong interest and investments from the industry as well, also including various non-medical-based applications. Precisely, the research on glucose detection systems is represented in various fields such as physics, chemistry, material science, and biotechnology, in the pursuit of the development of minimally invasive, miniaturized, and maximally sensitive sensors.

In our laboratories at IPE FME BUT, so far, sensors based on physisorption without the possibility of selectively distinguishing only one specific substance were studied. However, this work focuses on the selective detection of a single substance, glucose. As already mentioned, glucometers are the most common type of biosensors, so there is a wealth of information and studies enabling us to compare the results achieved by graphene sensors with others. Most frequently, glucose sensors work on the principle of selective reaction of glucose with the enzyme glucose oxidase (GOx). The same approach was implemented to develop our graphene-based glucose biosensor, which employs the GOx as a biological recognition element.

The device is designed to operate in two different setups and to respond only to the presence of glucose in the solution. The first setup employs a solution-gated graphene field-effect transistor (GFET) which utilizes graphene as the conductive channel across

it. The GFET is appropriate for the thorough electronic characterization of graphene. In addition to the detection of chemical and biological species, GFETs allow revealing their doping effects on the graphene channel, as well as the carrier mobility of graphene. The second setup is based on a straightforward resistance dependency of the GOx-functionalized graphene channel in response to different glucose concentrations. Hereby, the device enables continuous real-time monitoring of the glucose level.

1. Electrochemical biosensors

A biosensor is an analytical device capable of providing specific quantitative or semi-quantitative analytical information. A simple biosensor is shown in Fig. 1.1. It contains a biological recognition element (bio-receptor) that is either part of or in close contact with a physicochemical transducer, and electronics responsible for signal processing and display. The transducer transforms one signal into another one, which we can measure. The intensity of the generated signal (usually an electronic one) is directly or inversely proportional to the analyte concentration. The bio-receptor recognizes studied analyte up to the molecular level, which provides high sensitivity, specificity and the possibility of optimizing the sensor for a given analytical problem [1].

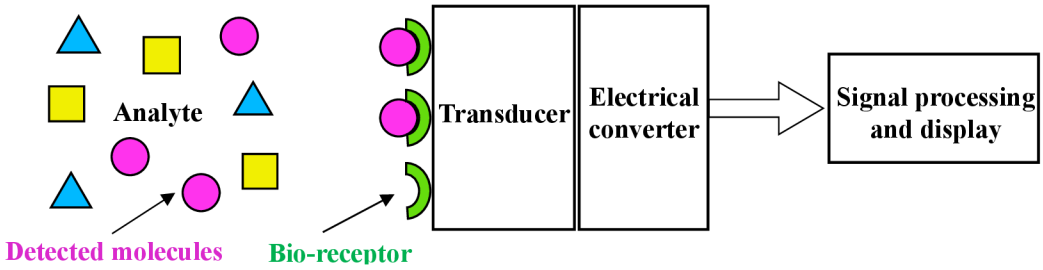

Figure 1.1: Scheme of a typical biosensor.

Biosensors can be divided according to bio-receptor or transducer elements, or their combinations. We select both of these elements by the type of measured physical quantity, the type of analyte under study and the properties of the sample. There are three predominant groups that classify **biosensors by the type of a biological recognition element**, i.e. biocatalytic, immuno and DNA sensors [2].

Biocatalytic sensors contain a bioelement that converts an analyte by chemical reactions. Such a reactive element comprise of one or more enzymes, whole cells, microorganisms (bacteria, fungi, yeast cell), or plant or animal tissue. Enzyme electrochemical biosensors are sought-after systems for efficient activity, specificity and simple, inexpensive instrumentation. The most commercialized proliferation of biocatalytic sensors is undoubtedly used for blood glucose monitoring.

Immunosensors operate on the principle of selective interaction with analyte. The interaction results in the formation of a thermodynamically stable bond between the analyte and an antibody, nucleic acid, or chemoreceptor. Immunosensors are highly specific, selective, and sensitive to the reaction of an antigen with an antibody. The most common immunosensor transducers are optical systems, in which interacting molecules are activated, for example, by imaging/labeling compounds, and piezoelectric systems.

DNA sensors are analogous to immunosensors and they contain defined DNA or RNA nucleic acid fragments. Upon delivery of an unknown nucleic acid to the immobilized fragment, base-pairing of the two elements occurs and generates nucleic acid structures.

Classification by the type of the physicochemical transducer is another characteristic to distinguish between individual biosensing systems. The transducer converts a certain physical quantity that is characteristic for each interaction between the analyte and biological element into a measurable signal by electrochemical, optical, piezoelectric, acoustic, or calorimetric methods. In this study, the emphasis is on the electrochemical biosensing system.

1.1 Electrochemical enyzamtic biosensor

The first electrochemical biosensor was introduced by Prof. Leland Clark in the 1960s and was designed to measure blood glucose [3]. The electrochemical biosensor is analytical device that transduces biochemical events to electrical signals, such as the reaction or interaction between a bio-receptor and analyte [4]. If we use an enzyme as a biological recognition component, we are talking about electrochemical enzyme sensors. In enzyme-catalyzed reactions, hydrogen peroxide is formed (except for water-forming oxidases) or oxygen is consumed (for all oxidases). The production and consumption of these substances can generally be described as:

$$Substrate + O_2 \xrightarrow{\text{Enzyme}} Product + H_2O_2. \tag{1.1}$$

Immobilization of the enzyme

The immobilization technique makes possible to fasten the biological material to parts of the sensor. In particular, it is essential to form a strong bond with the transducer element. The individual immobilization methods are summarized in the Fig. 1.2. Immobilization affects the function of the biosensor, mainly the reproducibility, stability, sensitivity and speed of response. The use of a suitable immobilization method depends on both the bioelement (enzyme) and the nature of the detection device and is essential for the fabrication of a useful biosensor [5].

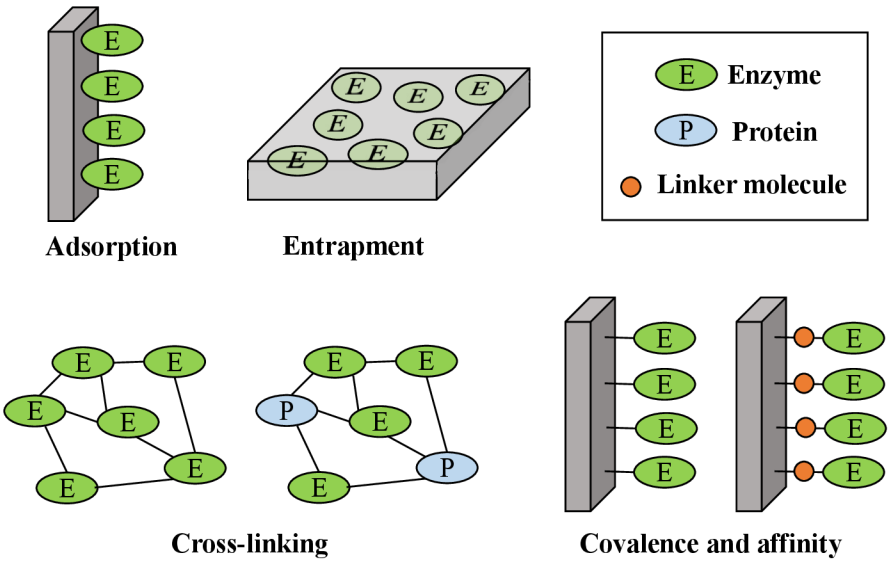

Figure 1.2: Schematic representation of the different methods of enzyme immobilization. Taken and modified from [6].

The classical physical absorption represents one of the simplest methods as it does not involve any functionalization and is non-destructive to the activity of the enzyme. Initially, enzyme is dissolved in a solution and the solid support is exposed to the solution for a fixed period of time. The enzyme molecules react with the surface under suitable conditions and adsorb on it. Subsequently, the unadsorbed residues are then washed away. Nevertheless, enzymes are loosely bound to the support by weak interactions such as van der Waal's and electrostatic interactions. Therefore, binding is more susceptible to changes in temperature, pH and ionic strength [6].

The entrapment is another physical method based on enzyme immobilization in 3D matrices such as electropolymers, photopolymers or silica gels. Again, it is one of the most stable and straightforward immobilization methods that does not modify the enzyme. However, one of the limiting factors is the possibility of the biomolecule leaching through the porous matrix, lower sensitivity and the reduced performance of the device due to the diffusion barriers [6].

The cross-linking means that the enzymes hold together either to each other or in the presence of another reagent. Such a strong bond is an advantage, but the chemical modification can lead to a loss of activity, since as a rule it is a linking *via* covalent bonds [6].

The covalent bonding or **the affinity interactions** offer stable complexes between enzymes and supports through chemical interactions. The support must be initially activated using coupling agents (functional groups). These groups are referred to as linkers and, in the case of organic linkers, they generally contain interacting -COOH, -NH_2, -SH, -OH terminal moieties[1]. The following enzyme incubation results in its binding to the activated surface through a strong bond with the reactive moiety of the linker. Such bonding is one of the most widely used methods, and has the advantage of allowing the control of the orientation and the amount of the immobilized enzyme on the surface. On the other hand, it is usually an irreversible method (change in the primary structure of the enzyme) that requires a great deal of effort in terms of the amount of reactans required and complex procedure. Moreover, it may be a challenge to determine whether the chemical bonding exactly took place or not, and some linkers may affect the activity of the enzyme [6, 7].

1.2 Glucose detection

In recent years, there has been a sharp increase in diseases of affluence worldwide, and one of the most common chronic diseases is diabetes mellitus. Therefore, research and development in the field of glucose detection has become of tremendous economic interest. Indeed, glucose sensors account for about 85 % of the entire biosensor market, making glucose the most commonly tested analyte[2]. For a healthy individual the

[1] covalent immobilization of enzymes include activation methods, such as: glutaraldehyde, epichlorohydrin, silane epoxide, cyanuric chloride, thiol silane+succinimide ester, chlorotriazine, carbodiimide, acyl azoture, carbonyldiimidazole, carbodiimide, or 2,2'-dipyridyldisulfur [6]

[2] other widely used biosensors include cholesterol testing, pregnancy testing, drug discovery, and today's conditional SARS-CoV-2 testing

blood sugar level is in the range of $4.4 - 6.6\,\mathrm{mM}$[3] and the metabolic disorder results in concentrations higher or lower than the normal range [8].

Nearly all current glucose biosensors are electrochemical as they exhibit high sensitivity, reliability and shelf-like stability. In addition, they exhibit a reasonable unit cost, convenient maintenance and reproducibility.

Enzymatic detection of glucose in the presence of the enzyme glucose oxidase has a long tradition, especially its determination using amperometric enzyme biosensors. These biosensors are characterized by good sensitivity and selectivity, however, many interfering substances in real samples can reduce these parameters. Impedance analysis is a very sensitive method detecting changes in capacitance and resistance in close proximity to the electrode. As such, it can therefore serve as an alternative to amperometric sensors, using the determination of changes in impedance parameters during the enzymatic conversion of glucose on the surface of an electrode with immobilized glucose oxidase.

Alternatives of non-GOx glucose sensing include glucose dehydrogenases, pyrroloquinolin dehydrogenases for direct electro-oxidation of glucose. However, these sensors often lack specificity and other sugars in the body such as lactose, galactose, maltose, cellulose, and xylose can interfere with the measurement [9].

Glucose

Glucose is one of the carbohydrates, which are the most common organic compounds, mostly of plant origin. Carbohydrates are formed primarily during photosynthesis in green plants from carbon dioxide and water by absorbing energy from the visible spectrum. Glucose is a simple monosaccharide from the group of aldohexoses containing six carbon atoms and an aldehyde group. Chemically pure glucose is a white crystalline substance with a sweet taste, commonly found in sweet fruits and other parts of plants. It occurs in two isomeric forms, the most common and naturally occurring being D-glucose (molecular projection in Fig. 1.3), while another form is a laboratory synthesizable L-glucose [10].

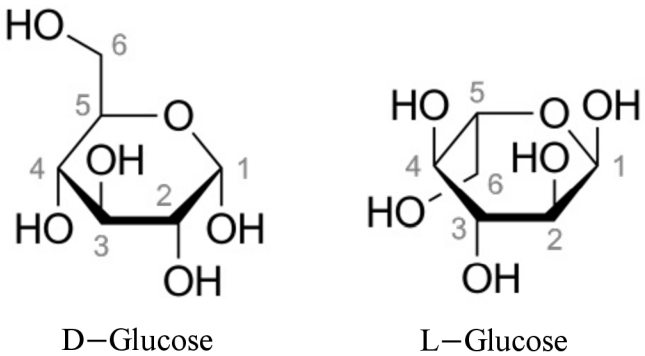

Figure 1.3: Haworth projection of D-glucose and L-glucose [10].

[3] the unit M of molar concentration corresponds to the SI unit $\mathrm{mol/m^3}$

Glucose oxidase

Thanks to its high selectivity, stability, and especially biocompatibility, the most widely used bio-receptor for glucose detection is glucose oxidase. Glucose 1-oxidase was discovered in 1928 by Müller and is most often obtained from *Aspergillus niger* fungus. It is an enzyme composed of two identical subunits (=dimer), which contains one flavine adenine dinucleotide cofactor per monomer, and a homodimer (a simulation of the structure of GOx dimer is shown in Fig. 3.6b). GOx is extremely stable in the lyophilized state (at 0 °C for 2 years, at −15 °C for 8 years). The stability is also dependent on the pH, with the highest stability at around pH 5, and the catalytic activity decline rapidly below pH 2 and above pH 8.

The glucose biosensor is based on the reaction between GOx and glucose molecules as shown in the following equation:

$$D - glucose + O_2 \xrightarrow{\text{GOx}} gluconic\ acid + H_2O_2 \tag{1.2}$$

The initial product of glucose oxidation is D-gluconolactone, which is a weak competitive inhibitor of GOx, but spontaneously hydrolyses to gluconic acid. The hydrolysis rate increases with increasing pH. Using glucose dehydrogenase, gluconolactone can be reconverted back to glucose. The first amperometric biosensors for glucose detection were based on oxygen consumption during the reaction shown in Eq. 1.2. Oxygen was detected at the cathode (usually Pt) *via* electrons generated from further reduction reaction $O_2 + 4H^+ + 4e^- \rightarrow 2H_2O$ following the equation 1.2 [3, 9]. This electrode is known as the Clark electrode [11].

Today, amperometric biosensors based on hydrogen peroxide formation are more commonly used, and compared to oxygen amperometric biosensors, they show higher sensitivity. Anodic oxidation of hydrogen peroxide then occurs at the electrode according to the equation:

$$H_2O_2 \rightarrow O_2 + 2H^+ + 2e^- \tag{1.3}$$

The electrochemically determined level of H_2O_2 is directly proportional to the amount of glucose [12].

Numerous methods have been used and others are evolving to **immobilize GOx** for the use in biosensing devices. The first biosensor using GOx was designed by Clark and Lyons in 1962 who demostrated the GOx immobilization *via* layers of semipermeable membranes [3]. Over the years, extensive research has been done on this issue, Tab. 1.1 presents a brief review of methods where GOx was immobilized on a carbon-based materials, such as a glassy carbon electrode, single- or multi-walled carbon nanotubes (CNTs), graphene.

Table 1.1 Glucose oxidase immobilization methods with carbon-based support materials.

Immobilization method	**Composite and support material**
Adsorption	GOx layer-by-layer adsorption with dendrimer-encapsulated Pt nanoparticles on CNTs [13]
	GOx adsorption on pyrolytic graphite [14]
Entrapment	GOx in silica gel on a glassy carbon electrode [15]
	GOx in the composite matrix for CNTs paste electrode [16]
	GOx in silk protein fibroin on a CVD graphene FET [17]
Cross-linking	GOx/bovine serum albumin mixture cross-linked with glutaraldehyde on carbon film [18]
Covalence and affinity	GOx covalent attachement on glassy carbon using the carbodiimide activation method [14]
	GOx covalently immobilized on CVD graphene through the linker molecules [19]

2. Functionalization of graphene

Graphene is a suitable candidate for application in biosensing, thanks to its high mobility of charge carriers and thermal stability. Unique electrical properties of graphene coupled with a specific recognition properties of a different biosystem immobilized on its surface would indeed make an ideal miniaturized biosensor. The graphene monolayer has a higher surface to volume ratio compared to any other material existing in nature, thereby, the binding of other atoms and molecules to its surface is of great interest.

A prerequisite for a wider application of graphene in this area is the development of chemical methods which immobilize biological molecules onto graphene in a reliable manner. This is the functionalization process, which allows the introduction of new characteristics from specific functional groups and could potentially pave the way for graphene's use in real biotechnological applications. However, the natural hydrophobicity of graphene after exposure to ambient air limits the binding of biomolecules to its surface[1] [20]. Therefore, in case of pristine graphene, linker molecules are frequently employed. Such initiator molecules attach to the graphene surface at one end and at the other end bind the functional biomolecule. Due to the strong hydrophobicity, the functionalization of graphene-based materials often employs the graphene oxide (GO) and reduced graphene oxide (rGO), which increase the hydrophilicity the presence of oxygen groups [4]. In this work, we focus on pristine graphene prepared by chemical vapour deposition (CVD), thus, functionalization methods of pristine graphene are introduced; covalent and non-covalent functionalization, and elemental doping.

2.1 Graphene

Graphene is a 2D carbon material with carbon atoms arranged in a hexagonal form. The sp^2 hybridized carbon atoms have bonds with three neighbours about 1.42 Å in distance. This three bonds are formed *via* σ bands as a result from the combination of s, p_x, and p_y orbitals. Furthermore, the fourth band, π band, is oriented outside of the plane and results from the p_z orbital. A free electron located in the π orbital can travel through the whole graphene which results in high electron mobility of around $1.5 \cdot 10^4\,cm^2\ V^{-1}\ s^{-1}$ characteristic of graphene. This is also known as a π-electron cloud and it comprises of a filled band of π orbital (called the valence band), and an empty band of π^* orbital (called the conduction band). The valence and conduction bands touch at the edge of the first Brillouin zone, thus, predetermine graphene as a zero bandgap material [22, 23]. For electronic sensors, completely or nearly pristine graphene can be obtained by three major methods, *i.e.* mechanical exfoliation, chemical vapour deposition, or reduction of graphene oxide.

The mechanical exfoliation method provides the highest-quality graphene and the process does not requiere any special equipment [26]. The principle of exfoliation

[1] the hydrophobicity is affected by unintentional hydrocarbon contamination from ambient air [20], moreover, the wettability of graphene is also significantly affected by the substrate [21]

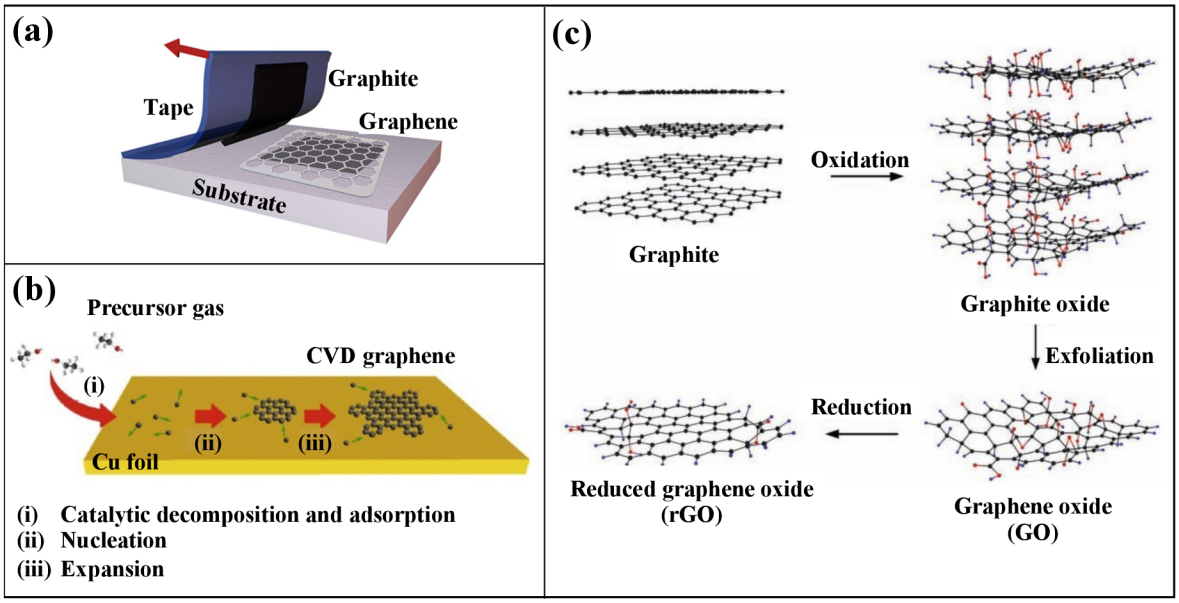

Figure 2.1: (a) Schematic representation of the mechanical exfoliation process. (b) Schematic representation of a CVD growth of graphene. Modified from [24]. (c) Synthesis route of rGO from graphite [25].

is the mechanical separation of graphene layers kept together by weak van der Waals forces in graphite using an adhesive tape (Fig. 2.1a). By this top-down approach, Novoselov et al. originally prepared graphene in the laboratory for the first time in 2004 [27]. Nevertheless, exfoliated pristine graphene is uncontrollable in shape, size and location, therefore, quite limited for the application in sensor devices [28].

Chemical vapour deposition is the most efficient method (cost, quality) enabling the production of large-scale graphene flakes. The principle of CVD (Fig. 2.1b) is the decomposition of hydrocarbons (methane, ethyne, ethene and others) into carbon atoms and their subsequent nucleation into a single-atom thick layer on a metal substrate (copper, nickel). Cu or Ni substrate is annealed in hydrogen and precursor hydrocarbon gases are pumped into a reaction chamber at elevated temperatures to grow a graphene monolayer [29]. Alternatively, the highly amorphous graphene films can be transferred to various substrates in the chosen device system. Due to well-defined growing conditions, the CVD graphene is highly suitable for application in nanoelectronics, and photonics. Functionalization is often conditioned by defect sites, while the CVD graphene is characterized by its high quality, the low reactivity and the resulting weak binding towards other groups happen to be limiting factors. Yet, defect sites can be partially adjusted by deposition parameters. The next important advantage of CVD graphene is relatively simple controlling of the doping concentration [19]. CVD graphene-based FETs can be employed as immunosensors [30], for the detection of exosomes by chemically modified graphene with antibodies [31], and for DNA sensing [32].

Reduced graphene oxide is prepared by reduction of GO sheets (Fig. 2.1c) by proposed strategies including chemical, thermal, electrochemical or photo-catalyzed

reduction, etc. [33] Hummer's method is the most used process for the production of graphite oxide from which the GO sheets are exfoliated. It uses strong acids and oxidation reagents ($NaNO_3$, $KMnO_4$, H_2SO_4) to oxidize graphite [34]. So far, complete reduction of graphene oxide has not been achieved. Residual hydroxyl and epoxy groups remain on the basal plane of rGO and degrade its conductivity compared to the pristine graphene. As a result, rGO is not suitable for microelectronic applications, but preferable for large-scale graphenic materials for instance requiring further modification. In addition to residual oxygen groups, the reduction process may leave behind defects as dislocations, therefore, the name rGO is used to distinguish it from pristine graphene. Nevertheless, thanks to the rich chemistry of such oxygen moieties their presence is favourable for consequent functionalization or reaction with analyte. Various functional groups can be linked to rGO through oxygen atoms. In this way, we must not forget the important role of graphene oxide itself. With a high density of hydroxyl, carboxyl and epoxy groups, GO enables the formation of a wide range of graphene derivatives, and thus, is versatile in applications in biotechnology and biosensing [35, 36, 37].

2.2 Covalent fuctionalization

As the name suggests, covalent functionalization occurs through a strong covalent bond, and it is associated with the electron sharing of the free out-plane electron. There are two general routes how to form the bond. First, the covalent bond can be performed using a C=C bond in the aromatic ring of graphene. The second way to form the covalent bond is through the bond between the oxygen group of rGO and the functional group. In general, it is more facile to perform this kind of functionalization on rGO or GO, as it contains oxygen groups which increase the binding as reactive defect sites. Such groups allow common chemical reactions to occur: isocyanation, carboxylic acylation, epoxy ring opening, diazation, and addition [38, 39, 40]. Nevertheless, in this study we focus on pristine graphene prepared by the CVD method and therefore the issue of rGO and GO functionalization will not be examined in greater detail.

The main methods of covalent functionalization comprise the cycloaddition reaction of free radicals[2] or dienophiles[3] to sp^2 carbon atoms of pristine graphene sheet. It provides stable and well-defined systems with tunable degree of functionalization. Free radicals include, for example, nitrophenyl [43], 4-propargyloxyphenyl [44] groups derived from diazonium salts, dienophiles include hydrocarbons which contain double or triple carbon-carbon bonds. Most commonly, free radicals are brought to graphene, where they react with the double C=C bond. As a result, a single C-C bond is formed and functional group binds covalently to carbon atoms. The interaction produces a considerable decrease of graphene's conductivity, as the orbitals of carbon atoms change from sp^2 to the sp^3 hybridization [38, 40]. In ref. [45], the covalent addition of phenyl groups to graphene (from the reaction of benzoyl peroxide), increased the level of hole doping. Such a graphene sheet was part of the GFET device, and the hole doping char-

[2] an atom, molecule, or an ion, usually highly chemically reactive, which contains an unpaired valence electron [41]

[3] a compound, usually an alkene or alkyne with an electron-withdrawing group which readily reacts with a diene in the Diels-Alder reaction [42]

acter was attributed to the physisorbed benzoyl peroxide. Similarly, $4-(2-(\text{pyridin-4-yl})\text{vinyl})\text{phenyl}$ group of a dye molecule[4] of a donor-π-acceptor structure was covalently coupled to graphene. Functionalization with the dye molecules induces the intramolecular charge-transfer and a bandgap modification of graphene [46].

Apart from free radicals, the sp^2 carbons of graphene can also participate in the Diels-Alder reaction, a chemical reaction between a conjugated electron-rich diene and an electron-poor dienophile. The interaction results in the addition of dienophiles to C-C bonds [47]. Graphene can be further decorated for example with dihydroxyl phenyl groups throught the pyrrolidine rings formed by the addition of dienophile azomethine ylide [48], or with porphyrin derivatives [49]. As well as azomethine ylide, diazonium salt, aldehydes or substituted α-amino acids can also serve as a precursor for the attachment of desirable functional groups. A covalent binding of radical initiator molecules by diazonium addition to rGO was performed by Fang et al. [50]. Although the rGO was employed, the oxygen groups did not participate in the binding of the molecules. Subsequently, by atom transfer radical polymerization, the initiator-grafted graphene sheets were further functionalized with linear polystyrene chains. Kwong et al. [31] modified CVD graphene on Si/SiO_2 substrate using a covalent linker 4-nitrophenyl diazonium salt. Here, the covalent character of the functionalization by the linker was confirmed by Raman spectroscopy.

2.3 Non-covalent fuctionalization

Methods for non-covalent functionalization of graphene, rGO, and GO include the $\pi-\pi$ stacking, electrostatic attraction, van der Waals forces, and hydrophobic-hydrophobic reactions. The resulting force arising from this interaction is a combination of attractive force as electrostatic, dispersive, and/or inductive interaction, and repulsive force as exchange repulsion. Unlike the covalent bonding, it does not rupture the conjugated network of graphene, and electronic properties are preserved. It is a pivotal interaction for the stabilization of proteins, enzymes, drug complexes, DNA-protein complexes, organic molecules, and functional nanomaterials, thus, of importance in device and sensing applications. A fer specific examples of non-covalent functionalizations of pristine graphene are further presented [40].

As far as pristine graphene is concerned, the predominantly used interaction of the functionalized group and the basal plane of graphene is *via* $\pi-\pi$ stacking. The $\pi-\pi$ interactions are associated with the interaction between the π-orbitals of graphene carbons and a molecular system. It favors the planarity of the interacting systems, hence, it is more convenient for the pristine graphene than rGO which exhibits deviations from the planarity. The interaction arises in three ways and can be explained by the interaction of two benzene rings, as shown in Fig. 2.2a-c. The first slipped (or offset) stacking, includes the benzene rings on top of each other but slightly displaced. The second edge-to-face (or T-shaped) stacking, contains two benzene rings in a perpendicular position, with a small possibility to occur around the edge of graphene sometimes terminated with a H atoms. The third and minor arrangement is a sandwich stacking,

[4] a highly π-conjugated chromophore with a pyridine moiety (acceptor) [46]

where C atoms are exactly on top of each other, creating a repulsion from overlapping π-cloud [40, 51].

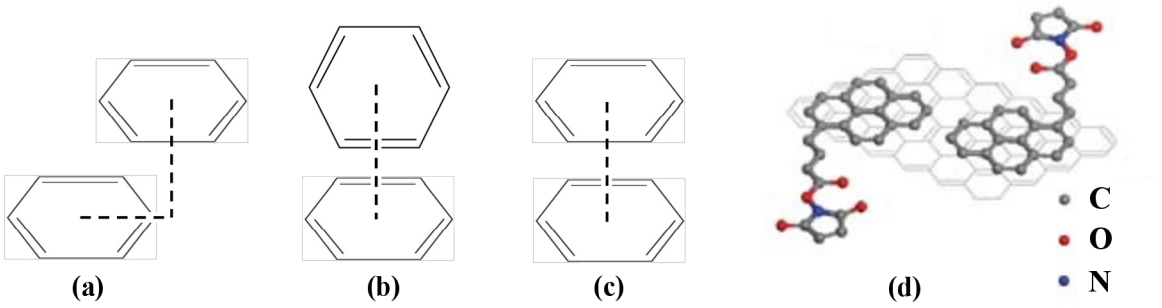

Figure 2.2: Representation of the $\pi-\pi$ stacking of benzene rings: (a) slipped, (b) edge-to-face, (c) sandwich type. (d) Chemical structure of the $\pi - \pi$ stacking of graphene and pyrene-containing molecule PSE [46]. Such stacking corresponds to the sandwich type, as reported in Ref. [52, 53, 54].

Negatively charged π-electron cloud of carbon atoms in graphene exhibits an attractive interaction with the π orbital of a functional group. The attractive electronic interaction occurs when the attractive interaction between the π-electrons and the σ-framework outweigh the usual contribution of a π-electron repulsion [51]. However, this attraction is predominated by a dispersion when the functional system has very similar electron density. To form a complex through the $\pi-\pi$ bond, it is necessary that one system has an abundance and the other a deficiency of electrons [40]. This allows small aromatic molecules such as pyridine and fluorinated benzene derivatives with aliphatic chains to bond onto graphene surface. Modifications of graphene through the $\pi - \pi$ interaction has been reported with perylene- and pyrene-terminal molecules. Molecules containing perylene include, e.g. pyrelene tetracarboxylic acid [55], perylene-tetracarboxylic dianhydride [56], and poly(N-isopropylacrylamide) [57]. In the case of pyrene derivatives, PSE [31, 52, 58, 59, 60, 61] is widely used to immobilize biomolecules with amino groups, such as proteins, peptides, amino-DNA and other molecules. In spite of that, Liu et al. [62] demonstrated the attachment with similar pyrene backbone structures: 1-pyrenebutyric acidic acid, 1-pyrenebutanol, 1-pyreneacetic acid, 1-pyrenecarboxylic acid and pyrene-1-boronic acid. The schematic representation of the $\pi - \pi$ stacking between graphene and pyrene-containing molecule PSE is represented in Fig. 2.2d.

Moreover, the $\pi - \pi$ stacking can be used directly to detect dopamine. Dopamine reacts selectively through $\pi - \pi$ interactions with graphene present on the electrodes of the sensor, and thus, does not interfere with ascorbic acid, which commonly occurs in dopamine detection [63].

Apart from the $\pi - \pi$ interactions, other significant non-covalent functionalizations of graphene involve the hydrophobic interaction between graphene characteristic for its hydrophobicity in ambient conditions and other hydrophobic or partially hydrophobic molecules. Such molecules have hydrophobic parts which interact with graphene

surface, and hydrophilic parts which interact with a solvent[5]. Consequently, the functionalization of graphene is mainly used to make graphene dispersive in solution systems (organic solvents or water). The technique can also serve for graphite exfoliation in the solution. The exfoliation is caused by functional groups penetrating between graphenic layers as wedges and attaching to nanosheets. Graphene nanosheets are gradually dissociated from each other and stabilize in the solution system [63].

2.4 Elemental doping of graphene

It should be added that the functionalization of graphene is performed not only for biosensing purposes, but also for tuning its electronic properties. Herein, a brief review is given on the matter of chemical doping of graphene, which may result in electron doping of graphene, band gap opening and/or change of the electrochemical properties. Chemical doping occurs when the graphene lattice interacts with atoms of a different chemical composition. Two types of chemical doping are distinguished; **substitutional doping**, when a carbon atom of a graphene lattice is replaced by another atom, or **adsorption-induced doping**, when atom/molecules exchange electrons with graphene and adsorb on its surface.

Boron and nitrogen are the best candidates for substitutes into the honeycomb graphene lattice, as they have atomic sizes similar to carbon and the number of electrons differs by one compared to C. Boron exhibits an electron acceptor characteristic (p-type doping), while nitrogen exhibits an electron donor characteristics (n-type doping). Such incorporation of foreign atoms disrupt the sp^2 hybridization of C atoms, thus, leads to a Fermi level shift and to the opening of the band gap. The Fermi level of graphene is driven below the Dirac point for p-type doping, whereas, n-type doping drives the Fermi level above the Dirac point.

Compared to the substitutional doping, the adsorption-induced doping does not disrupt the structure of graphene and is usually reversible. n-Type doping occurs when the highest occupied molecular orbital (HOMO) of the dopant is above the Fermi level of graphene[6]. On the contrary, p-type doping occurs when the lowest unocuppied molecular orbital (LUMO) of the dopant is below the Fermi level of graphene[7] [64, 65].

Characterization of the functionalization

In this work, Raman spectroscopy and atomic force microscopy were used as characterization tools of the functionalization. These techniques are routinely used to obtain information regarding the number of layers, the quality, effects of perturbations, and surface morphology of graphene [66]. In the following paragraphs, their principles will be briefly explained.

Principle of Raman spectroscopy

Raman spectroscopy is a non-destructive method of studying the composition of substances that differ on the basis of bonds between atoms. The basic principle of Raman

[5] e.g. surfactants, ionic liquids or macromolecules
[6] applies to molecules with electron donating groups
[7] applies to molecules with electron accepting groups

spectroscopy is the inelastic scattering of monochromatic light from a laser. The laser photon interacts with vibrations of molecules, lattice oscillations (phonons) and other excitations, as a result of which the energy of the photon decreases or increases. Most often, the photon transfers energy to the electron, which excites it to a higher energy level. When the electron returns to the original level, it emits a photon with the same energy (and the same wavelength) as the original photon. This elastic scattering is called Rayleigh scattering and is not significant for the analysis of the Raman spectrum itself. Inelastic Stokes and Anti-Stokes scattering are of major importance for the analysis of information from the Raman spectrum. During Stokes scattering, after excitation, the electron returns to a higher energy level than from which it was excited. During deexcitation, a photon emits at lower energy (and higher in wavelength) than the original photon. Anti-Stokes scattering is less likely, in which the electron returns to a lower energy level during deexcitation and emits a photon with a higher energy (and smaller wavelength).

The difference between the energy of an incident and an emitted photon is the energy that has been transferred to the molecules for the transition between individual vibrational states, phonon interactions and for other crystal lattice phenomena. According to the measured energy entering back into the microscope, it is possible to characterize the molecules [67, 68].

Principle of atomic force microscopy

Atomic force microscopy is one of the most widespread scientific techniques for examining the morphology of solid surfaces with high resolution. The technique uses specially made needle-shaped tips with a tip of a few nanometers. The distance between the tip and the sample is between 0.1 and 10 nm and can be controlled with an accuracy of up to 0.01 Å.

In AFM, the interaction of the tip with the surface is characterized by means of a force acting between them (van der Waals forces, capillary forces, chemical bonds, electrostatic forces). The force is proportional to the distance between the tip and the sample surface. Quantitatively, the force interaction between two neutral atoms can be approximated by the Lennard-Jones potential, which is based on the van der Waals-London interaction representing the attractive component, and Pauli's exclusion principle, which is the repulsive component. When the tip-surface distance is changed, the force deviates from its initial value. The feedback system removes this deviation with the added signal and records its value. The computer then draws a topographic image of the surface from the signal recorded during the scan [68, 69].

3. Biosensor based on graphene field-effect transistor

Field-effect transistors (FETs) are primarily used as amplifiers or logical switches. In case of switches, the channel material (semiconducting) must have a high on/off ratio of the flowing current. In other words, a sufficient difference between the on-state current and off-state current must be achieved when a switching gate voltage is applied. Thus, the conductive channel material should have a band gap between the conduction and valence bands enabling the decrease of its conductance. GFETs consist of graphene, known for its zero band gap, employed as the conductive channel. In this regard, several approaches have been introduced to open its band gap enabling it to turn its conduction on or off. A well-known method is to break the symmetry of the graphene structure, for example by forming graphene narrowings, bilayers, or by substituting carbon atoms in graphene with other atoms or molecules.

In graphene-based sensors, the on-off ratio is not as critical as in logical units, and GFET works more like amplifier. Moreover, thanks to the combination of high carrier mobility and sensitivity to surface effects of graphene, GFETs are an encouraging approach to such sensor devices. In combination with the specificity provided by the functionalization of graphene, GFETs hold tremendous promise for application in biosensors. In such a device, the graphene channel represents a transducer, thus, a key component for the immobilization of a biological recognition element (enzymes, antibodies, or nucleic acids).

3.1 Principle of GFET

As the name suggests, in a field-effect transistor, we control the current flow of charge carriers in the channel by applied transversal electric field. The current is carried by only one type of charge carrier (electrons or holes), hence its other name, unipolar transistor. Compared to bipolar transistors, the FET device allows a high-frequency response. A FET consists of a semiconducting channel, and three electrodes: drain (D), source (S), and gate (G), as illustrated in the diagram of a general FET, shown in Fig. 3.1a. A current flows through the channel that is insulated from the gate electrode and placed between the source and the drain. An applied voltage V_{DS} between D and S results in a flow of charge carriers through the conductive channel. Applied gate voltage V_{G} modulates the charge carrier density of the channel, and enables to control the output drain-source current I_{DS}. For the case in Fig. 3.1a, the FETs channel is an n-type semiconductor, and electrons are majority charge carriers [70, 71].

A special type of FET is a graphene field-effect transistor (GFET). A fundamental three-terminal GFET is similar to the conventional FET, where the conductive channel consists of graphene. GFET takes advantage of the fact that charge carriers can be induced in graphene by an application of gate voltage. This generates an electric field in the insulating region between the graphene channel and the gate electrode. By

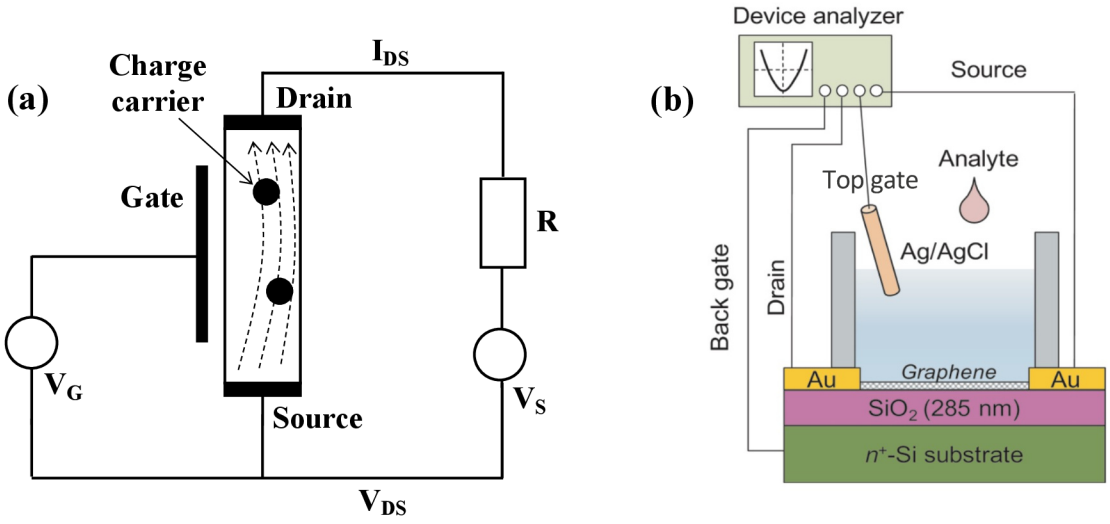

Figure 3.1: (a) A general diagram of the field-effect transistor. Taken and modified from [71]. (b) The typical GFET with solution-based isolation of gate electrode used in bioanalytical sensor [72].

the gate voltage, it is possible to change the type and charge carrier density in the graphene channel. Electrons in graphene channel are induced by positive gate voltage, while holes are induced by negative gate voltage.

3.2 Characteristics of GFET-based biosensor

A GFET based sensor consists of a graphene channel placed on a non-conductive substrate layer (e.g., SiO_2, polymers, etc.) between D, S electrodes. The G electrode can be assembled in back-gate, top-gate, or combined configuration that is shown in Fig. 3.1b. Considering the detection of biological samples, GFETs generally operate in the top-gate configuration[1]. Such an arrangement is also referred to as a solution-gate regime since the gate electrode (usually Ag/AgCl, Ag, or Pt wire) is immersed in a media containing the target molecules (electrolyte).

The graphene channel serves as a transducer element of a biosensor and is responsible for the transport of electrical current. At the same time, it serves as a support for the biological recognition element (bio-receptor). The detected molecules from the analyte adsorb onto the recognition layer and react with bio-receptor molecules. This alters the charge carrier density in the channel and results in alternations of GFET's electrical characteristics, and provides information about detected molecules. For the modulation of density and polarity of charge carriers in the graphene channel, a potential is applied at the G electrode. In the electrolyte, an electric-double layer (EDL) formed by the redistribution of ions in the medium acts as an insulator separating the gate from the channel. Depending on the method of measurement, we observe differences in either the drain-source current or the drain-source voltage, commonly computed to resistance (or conductance).

[1] in a back-gate configuration the conductive bottom substrate acts as the G electrode, this type is favored as a gas sensor [70]

The top-gate setup is also more advantageous for biosensors, since the solution isolating the gate electrode can incorporate a detected biochemical substance. To prevent current leakage from ionic conduction, S and D electrodes are commonly insulated from the analyte solution. As for the insulating material, polydimethylsiloxane (PDMS), poly(methyl methacrylate) (PMMA), silicone rubber, SU-8 resist, and other epoxy-based polymers are frequently employed [32, 70, 73, 74].

Electrical characterization

The detection mechanism of the GFET biosensor is based on changes in electrical metrics of the graphene channel induced by changes in the analyte solution. Changes in the density of charge carriers include the generation of charge carriers (when the drain-source current increases), or the reduction of the change carrier mobility (drain-source current decreases). Moreover, the charge carrier mobility similarly influences the drain-source current. However, in case of adsorption of molecules at the surface, the influence of charge carrier density is dominant. In biosensing applications, the effects of the biological sample can be monitored by two approaches: by comparing the electrical transfer curves before and after exposure to the sample, or by dynamic real-time detection [70]. Three standard curves characterizing the GFET device are shown in Fig. 3.2-3.4, including examples from experiments performed by GFETs glucose biosensors based on CVD-grown graphene from previous studies [17, 19].

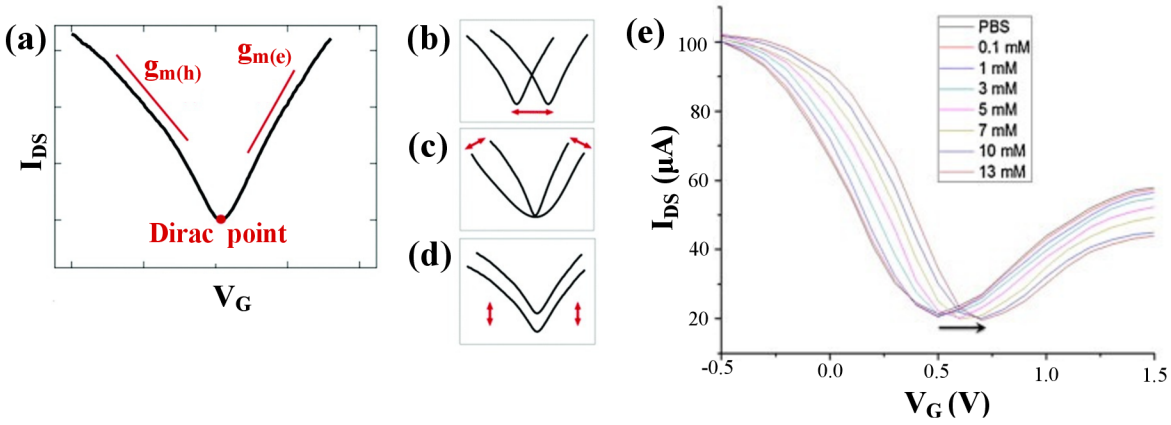

Figure 3.2: (a) A typical V-shaped transfer curve of a GFET, I_{DS} as a function of V_{G}. The left branch (p-branch) represents an increasing density of holes, whereas the right branch represents the increase of electron-density. The key characteristics of GFET sensor: (b) shift of the Dirac point depending on the doping effect induced to the channel, (c) change in the transconductance of holes $g_{\mathrm{m(h)}}$ or electrons $g_{\mathrm{m(e)}}$ corresponding to the mobility, (d) change in the output current amplitude, including the Dirac point. Taken and modified from [70]. (e) Charge transfer curves of GOx functionalized GFET in response to a glucose solution of various concentrations at $V_{\mathrm{DS}} = 100\,\mathrm{mV}$ (the units mM refer to a molar concentration $10^{-3}\,\mathrm{mol/L}$). GOx molecules were entrapped in silk protein. Taken from [17].

The transfer curves (Fig. 3.2) represent the output drain-source current I_{DS}[2] as a function of the gate voltage. It is obtained by sweeping the gate voltage V_{G} while

[2] or resistance as $R_{\mathrm{DS}} = V_{\mathrm{DS}}/I_{\mathrm{DS}}$, or conductance $G_{\mathrm{DS}} = 1/R_{\mathrm{DS}}$

maintaining a fixed drain-source voltage V_{DS}. Graphene exhibits a characteristic V-shape transfer curve representing the bipolar behavior of the field effect. An important feature of the transfer curves is the Dirac point[3], which indicates the minimum density of charge carriers - and thus minimum conductance. In GFET, the Dirac point divides the curve into two branches according to the type of the majority charge carriers in the graphene channel (at the DP, the populations of holes and electrons are equal).

Furthermore, the curve can be characterized by the slope g_m of the linear part of the p- or n-branch. The slope is called the transconductance and is given by:

$$g_m = \frac{W}{L} \mu C_{Tot} V_{DS}, \tag{3.1}$$

where W and L are the width and length of the graphene channel, respectively. μ is the mobility of charge carriers, and C_{Tot} the gate-electrolyte (here denoted "total") capacitance. The total capacitance for solution-gate GFET is commonly determined using the capacitance of an EDL in the electrolyte solution at the graphene surface and quantum capacitance of the graphene layer [70].

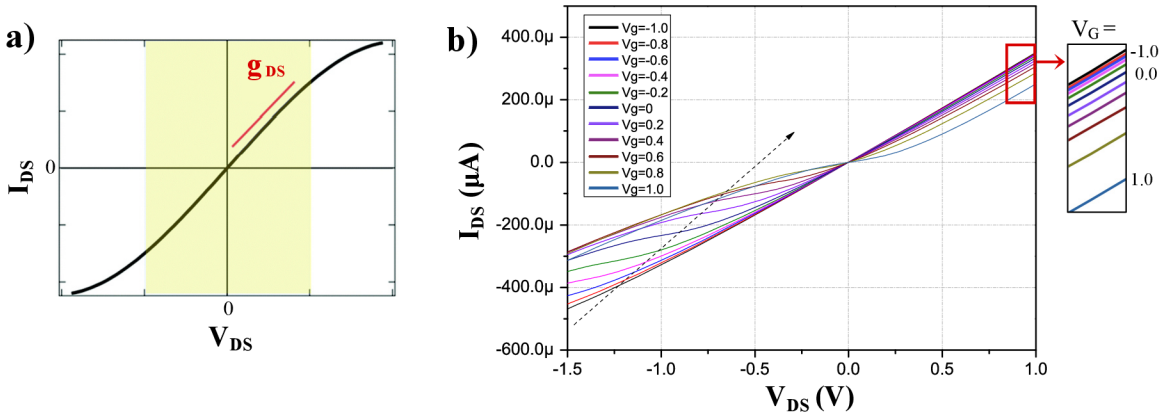

Figure 3.3: (a) A typical output curve of a GFET, I_{DS} as a function of V_{DS} at a fixed V_G. The amplitude of the drain-source current increases with the applied drain-source voltage, g_{DS} represents the slope of the output conductance. The yellow area represents the expected linear regime. Taken from [70]. (b) The output curve of a GFET from Ref. [19], utilized as a glucose sensor. The graphene channel was functionalized by GOx through a linker molecule PSE. V_{DS} as a function of drain-source current I_{DS} with the variation of V_G from -1.5 to 1 V. The dotted arrow shows the direction of the shift in the Dirac point.

The output curve, illustrated in Fig. 3.3, represents the output drain-source current I_{DS} as a function of the drain-source voltage V_{DS}. The gate voltage V_{DS} is fixed at a constant value. As the applied V_{DS} increases, the output current increases. For a very high quality design, i.e. a high quality graphene layer, electrodes, and mutual contacts, the output curve is expected to have a linear shape at low gate voltages.

For the detection of biological analytes in real time, the evolution of the output

[3] or charge neutrality point

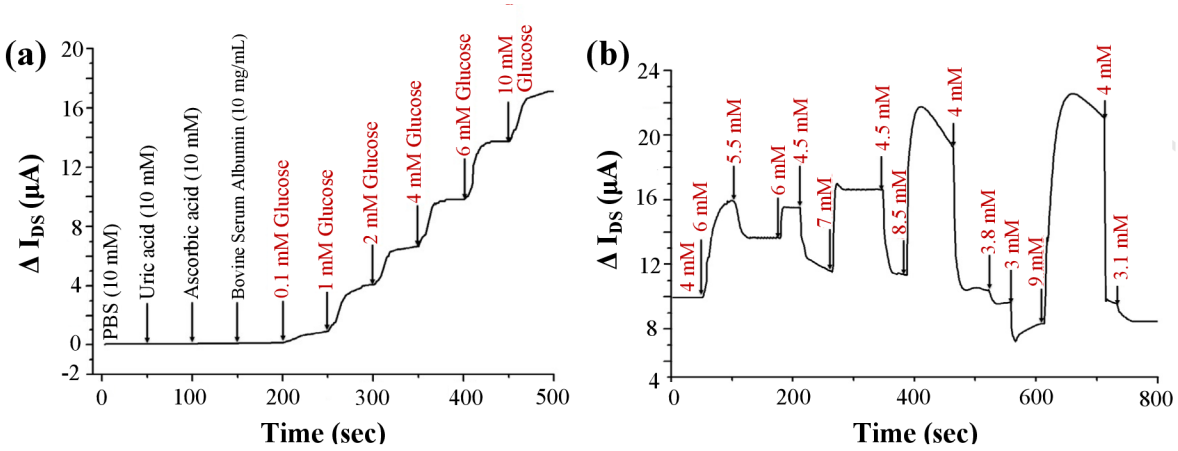

Figure 3.4: The real-time drain-source current I_{DS} measurement of the silk/GOx functionalized GFET glucose sensor from Ref. [17]. (a) The current responses to the addition of interfering substances, such as uric acid, ascorbic acid, and bovine serum albumin, and to the sequential addition of glucose from 200 s. (b) The current responses to the glucose solution of various concentrations (in mM) at a fixed $V_{\mathrm{G}} = 0\,\mathrm{V}$.

drain-source current I_{DS} (for a fixed gate voltage) is monitored as a function of time (Fig. 3.4). The analyte solution containing detected molecules is injected during the measurements to reach a desired concentration. The advantage of real-time measurements, is the ability to immediately test the selectivity of a given sensor when exposed to other interfering substances, as shown in Fig. 3.4b [70].

Mobility of GFET

In the solution-gate GFET, the electrical double layer works as a top-gate dielectric layer. This double layer forms between graphene and the solution at the graphene-solution interface when a voltage is applied to the gate electrode. The value of the charge carrier mobility μ may be approximated and indicates the ability of the carrier (hole and electron) to drift in a material depending on the applied electric field[4]. First, we define the area of graphene that will be exposed to the electrolyte and consider it as a metal disc of the radius r. Then, the capacitance of the dielectric layer formed between graphene and electrolyte interface (EDL), $\mathrm{C_{EDL}}$ is given by equation [19]:

$$\mathrm{C_{EDL}} = \frac{2\pi\epsilon_0(\epsilon_\mathrm{r}+1)r}{\tan^{-1}(2h(\epsilon_\mathrm{r}+1)/r\epsilon_\mathrm{r})}, \tag{3.2}$$

where h, ϵ_0, ϵ_r are the thickness of the EDL (usually in the range of Å to a few nm), the vacuum permittivity, and the relative permittivity of the electrolyte solution, respectively [19, 61, 72, 75]. Since the arrangement corresponds to capacitors in series, the total solution-gate capacitance ($\mathrm{C_{Tot}}$) can be calculated by the following equation:

$$\mathrm{C_{Tot}} = \frac{\mathrm{C_{EDL}C_q}}{(\mathrm{C_{EDL}} + \mathrm{C_q})}, \tag{3.3}$$

where $\mathrm{C_q}$ is the quantum capacitance of the graphene layer [19, 72]. In the linear

[4] the drift velocity is calculated as: $v_\mathrm{d} = \mu E$, where E is the applied electric field

regime of the transfer characteristic, the mobility μ for electrons and holes is given by:

$$\mu = \frac{\Delta\sigma}{\mathrm{C_{Tot}}\Delta\mathrm{V_G}} = \left(\frac{\Delta I_{\mathrm{DS}} L}{V_{\mathrm{DS}} W}\right) / (\mathrm{C_{Tot}}\Delta V_{\mathrm{G}}), \tag{3.4}$$

where $\Delta\sigma, L, W, \Delta I_{\mathrm{DS}}, V_{\mathrm{DS}}$, and ΔV_{G} are the differential conductance, the length and the width of the channel, differential drain-source current, drain-source voltage, and differential gate voltage, respectively [19, 76, 77].

Fermi level shift of graphene

For pristine graphene, the Fermi level (E_{F}) is located at the Dirac point. Once the graphene is doped, the Fermi level shifts away from the Dirac point. The Fermi level shift (ΔE_{F}) is defined as the energy difference between the Fermi level and the Dirac point. For the p-doped graphene, the Fermi level is below the Dirac point due to electron-accepting groups adsorbed on graphene. In case of p-doped graphene the Fermi level is above the Dirac point, and electron-donating groups are introduced [78].

In GFET, the Fermi level shift of graphene can be estimated from the electrical measurements as:

$$\Delta E_{\mathrm{F}} = -sgn(n) \cdot v_{\mathrm{F}} \cdot \hbar \cdot \sqrt{\pi \cdot |n|}, \tag{3.5}$$

where v_{F} is the Fermi velocity of graphene, $\hbar$ is the reduced Planck constant, and n is the charge-carrier density (positive for holes, negative for electrons). In a solution-gate GFET, the carrier density of graphene is estimated by the following equation:

$$n = \frac{\mathrm{C_{Tot}} \cdot V_{\mathrm{DP}}}{e}, \tag{3.6}$$

where $\mathrm{C_{Tot}}$ in the total capacitance from Eq. 3.3, e is elementary charge, and V_{DP} is the gate voltage at Dirac point [61, 79].

3.3 Glucose GFET biosensors based on GOx

The majority of glucose sensors utilize the selective reaction of glucose with glucose oxidase. The reaction cycle adapted for graphene employed as the transducer element is illustrated in Fig. 3.5. Glucose is converted to gluconolactone, while the enzyme GOx is reduced and cycles back by producing hydrogen peroxide. The oxidation of the latter is catalyzed at the graphene surface and the current measured is proportional to the glucose concentration. In GFET devices, the change in the potential drop at the gate/electrolyte interface caused by the reaction cycle in Fig. 3.5 is accompanied by a change in the gating of the channel in a manner that allows for the determination of glucose concentration [80].

A key step of the fabrication of GFET glucose biosensors is to immobilize the bio-recognition element GOx to the surface of the graphene channel. For example, Shin et al. [81] demonstrated glucose sensor based on palladium nanoflower decorated CVD graphene combined with GOx and Nafion functionalization. The sensor showed high selectivity and an exceptionally high sensitivity with a minimum detectable level up to 1 nm. Nevertheless, the main approaches to GOx immobilization when used in GFET

sensors adopt a stable attachment of GOx molecule *via* linker PSE[5] (Fig. 3.6b), or entrapment of GOx in a compound.

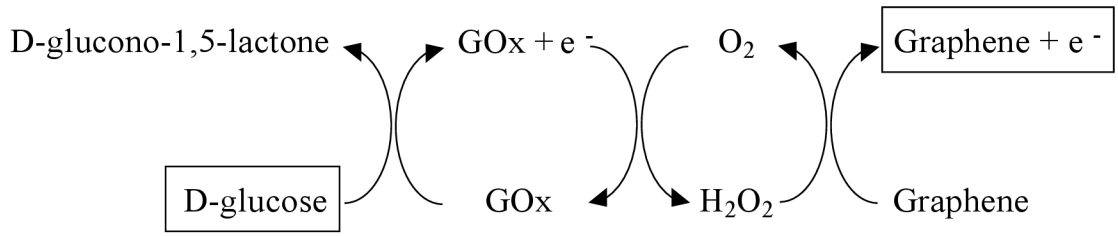

Figure 3.5: Reaction cycles for detection of glucose in devices utilizing a graphene electrode. Modified from [80].

Immobilization of GOx by the linker PSE

In 2001, Chen et al. [82] presented the immobilization of proteins on single-walled carbon nanotubes[6]. The sidewalks of CNTs were functionalized with the linker 1-pyrenebutanoic acid succinimidyl ester in a non-covalent way. This treatment preserves the essential electrical characteristics derived from the sp^2 CNTs electronic structure, given by their building block graphene. The PSE molecules dissolved in an organic solvent (DMF = dimethylformamide or methanol) irreversibly adsorb onto the hydrophobic surface of CNTs. Fig. 3.6a shows the linker PSE decomposed into constituent parts. The highly aromatic pyrenyl group of PSE creates $\pi - \pi$ bond with CNTs' sidewalks and thus provides a stable fixation. Fig. 2.2d illustrates the linker PSE attached to the surface of graphene. The succinimidyl groups of PSE are highly reactive and tend to form a stable amide bond with most proteins through the nucleophilic substitution of *N*-hydroxysuccinimide ester end by an amine group in the protein.

To perform the functionalization of graphene-like materials, the samples are incubated in a 1-pyrenebutanoic acid succinimidyl ester solution. In this study [82], authors incubated CNTs in 6 mM PSE solution in DMF, or in 1 mM PSE in methanol, for 1 h at room temperature. Later, the PSE functionalization process suitable for graphene was investigated. Wu et al. [83] showed that the dominant factor for PSE functionalization is the incubation time, not the concentration of the PSE solution. Additionally, after a long incubation time, the interaction between graphene and PSE saturates. Thereafter for graphene, the combination of 5 mM concentration and incubation time of 2 hours became widely utilized. The incubation is then followed by rinsing in pure DMF (alternatively methanol or isopropyl alcohol) and deionized water to remove excess unbound PSE residues.

The initial successful functionalization of the CNTs by PSE was followed by Besteman et al. [59], who introduced further immobilization of the GOx enzyme *via* the linker PSE (Schematic representation of such immobilization is shown in Fig. 1.2). On one side the linker PSE binds to the single-walled CNT through van der Waals coupling,

[5] the same approach was implemented to develop our graphene-based glucose biosensor
[6] which are basically graphene sheets rolled up into tubes

and on the other side binds covalently to the GOx enzyme. Such a functionalization was confirmed using AFM. After the addition of GOx, the height of PSE-modified CNTs increased for $1 - 4$ nm which is in good agreement with the height of dry GOx. The authors examined the electrical properties of CNTs in a solution-gate configuration during individual steps of functionalization, and confirmed that the non-covalently bound linker alone did not affect the conductance of the CNTs-based device channel. The subsequently attached GOx significantly reduced it, which was attributed to a change in the capacitance of the tube, rather than a simple electrostatic interpretation. Another feature brought by GOx is a strong pH-dependent conductance of the channel for pH values in the range of $4 - 5.5$. Furthermore, the effect of glucose (in the form of a solution in deionized water) on the conductance of GOx-functionalized CNTs was tested. During a real-time electronic response measurement, an increase of conductance associated with glucose addition has been proved (change of 10 % for 0.1 M glucose solution). Such an increase is the result of the selective reaction of glucose with GOx, since the uncharged glucose is unlikely to change the tube-electrolyte double-layer capacitance[7]. This paved the way for further research into biosensors based on graphene-like structures with biomolecular immobilization, including glucose sensors with immobilized GOx.

1-Pyrenebutanoic acid succinimidyl ester (PSE)

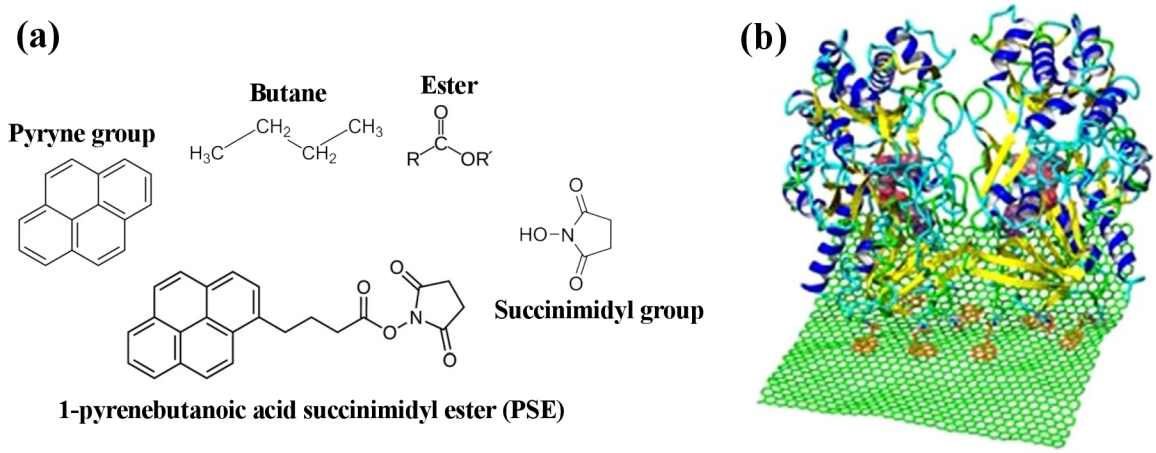

Figure 3.6: (a) The linker PSE decomposed into constituent parts. R denotes alkyl or aryl group or hydrogen, R' denotes alkyl or aryl group. (b) A molecular dynamics simulation of GOx dimer bound to the graphene surface *via* linker PSE (orange). Taken from [84].

Since the non-covalent functionalization approach by PSE is the least disruptive of the surface orbital structure of graphene, it proves to be the best choice in situations when one wishes to best retain the electronic properties of pristine graphene. Therefore, additional information are introduced about the PSE linker molecule.

The yellow solid polyaromatic hydrocarbon PSE is soluble in organic solvents such as chloroform, *N*,*N*-dimethylformamide, dimethyl sulfoxide, and methanol [85]. In the

[7] this was confirmed by the fact that the conductance of unmodified graphite electrode did not show any changes after the addition of glucose

view of the fact that graphene structure is considered as an infinite aromatic molecule, after PSE functionalization, it adopts parallel stacking on its surface, as demonstrated on the benzene rings in Fig. 2.2a, b. The aim is to maximize the graphene-PSE interaction, since PSE has four $\pi - \pi$ binding sides [61]. The binding of PSE to CNTs was investigated by AFM; measurements performed before and after PSE functionalization showed the height difference $2 - 3\,\text{nm}$ [86]. However, in Ref. [62], the thickness of the PSE layer on the CVD graphene sheet was determined as $\sim 0.7\,\text{nm}$ due to the self-terminating ability of the PSE linker. Moreover, the spacing of PSE-graphene stacking, i.e. graphene C atoms and the pyrene group of PSE molecule, was determined by DFT calculations as 2.3 Å [62].

Han et al. [87] investigated the background of the structural details and the non-covalent adsorption of PSE onto graphene sheet. Based on enthalpy calculations on minimized structures, the study presented that two optimal packing configurations are favourable, one at the density of one PSE per 24 graphene atoms and one PSE per 40 graphene atoms.

The doping effects of PSE on graphene were investigated by monitoring the shift of Dirac point voltage and by DFT calculations in Ref. [61], and [62], respectively. The results show that because of its electron-accepting property, the PSE imposes a p-doping effect on graphene. Calculations of the partial density of states have shown that the p orbital of C atom in the graphene lattice and the s orbital of nearest H atom in PSE molecule are slightly hybridized.

Over and above the immobilization of functional groups, the PSE exhibits fluorescence in blue range of the spectrum, thus, is commonly used as a fluorescent dye for labeling applications, or to create environment-sensitive bioconjugates. Furthermore, it is used for the characterization of cyclodextrin-based polyrotaxanes, the detection of nucleic acids, polyamines, probing lysozyme in human serum, and as a substrate for measuring polymerases, recombinases, topoisomerases activity [85].

Immobilization of GOx by the linker PSE

In 2014, You et al. [17] presented another approach to GOx immobilization on CVD graphene which consisted of GOx entrapment. For the biosensor to be sufficiently flexible, mechanically robust, easy to prepare, and biocompatible, the CVD graphene channel was coated with a compound of GOx and a silk protein fibroin. The silk protein was employed as both the GOx immobilizer and the substrate element. The assembly of silk fibroin results in localized nano-scale pockets where enzyme could be entrapped[8], as shown in Fig. 1.2b.

One year later, Zhang et al. [89] introduced a whole-graphene FET sensor, in which CVD-grown graphene was used as both the channel and the gate electrode. The gate electrodes were modified with GOx entrapped in biocompatible polymers including chitosan and Nafion. The device showed a detectable range from 0.5 mM to 1 mM, suitable for the detection of glucose in body fluids, in which the glucose levels are much lower that in plasma.

[8] similarly, Lu et al. [88] reported that silk fibroin can maintain enzyme activity for over 10 months

3.4 State of art

In 2010 Huang et al. [60] presented a GFET biosensor for the detection of glucose molecules based on functionalized CVD-grown graphene. Large-sized graphene placed on a quartz substrate was functionalized with the enzyme GOx immobilized on its surface by the intermediate linker PSE (represented in Fig. 3.6b). The authors introduced a successful procedure for the functionalization of GFET, which became a model for further development of such a sensor, including ours. First, the graphene device was incubated with a solution of PSE in DMF. After this modification, it was incubated overnight with GOx in a phosphate buffer (PBS). AFM images of graphene film before and after the complete functionalization confirmed a good enzyme coverage of the graphene sheet.

Glucose molecules were detected in the FET configuration of the sensor *via* V_G applied on Ag/AgCl solution-gate electrode. Transfer curves (I_{DS} *vs.* V_G) showed an increase in graphene conductance and a slight shift of the Dirac point indicating the p-doping effect of glucose. Since graphene was initially p-doped, it denoted that electrons generated from the oxidation reaction were not detected, but rather its product, hydrogen peroxide. On the other hand, when exposed to gluconolactone (another product of the glucose-GOx reaction) the channel's conductance did not undergo any changes.

Real-time detection measurements[9] (I_{DS} vs. *time*) were performed at constant drain-source voltage V_{DS} and zero gate voltage V_G, while the drain-source current I_{DS} was continuously monitored. Glucose was gradually added to the analyte reservoir with a PBS solution, causing an increase of the I_{DS} upon higher concentrations.

Two years later, Kwak et al. [19] demonstrated a similar glucose GFET sensor placed on a flexible, durable, and biocompatible substrate polyethylene terephthalate (PET). The experimental apparatus of the sensor is shown in Fig. 3.7a. At the two opposite ends of the CVD-grown graphene film, drain and source electrodes were placed, which consisted of conductive silver paint. To maintain the same active area of the sensor's surface, a well made out of polydimethylsiloxane (PDMS) was attached on top of the graphene channel. Platinum wire was used for the top solution-gate electrode. The applied gate voltage induces the adsorption of ions on the graphene surface, which modulate the graphene channel conductance.

First, the hydroxide peroxide (H_2O_2) was detected, as it is the final product of the reaction of glucose and GOx (reaction in Eq. 1.2). The measured range of H_2O_2 concentration was between $0 - 4\,\text{mM}$, and for higher concentrations, the Dirac point shifted to lower V_G (Fig. 3.7b). Such a shift indicates the n-type doping character of H_2O_2 due to the direct electron transfer on the graphene surface.

Fig. 3.7b shows the transfer curves for glucose detection at a fixed value $V_{DS} = -0.2\,\text{V}$. As well as for H_2O_2, the Dirac point shifted towards lower V_G upon the increasing glucose concentration. The measurable range of the sensor was from 3.3 to 10.9 mM of glucose, mostly covering the reference range of medical examination for diabetes diagnostic. Detection of glucose was performed on samples with flat and bent PET substrate and both showed similar behavior of the transfer curves. Nevertheless, the

[9] also called time series, or continuous monitoring

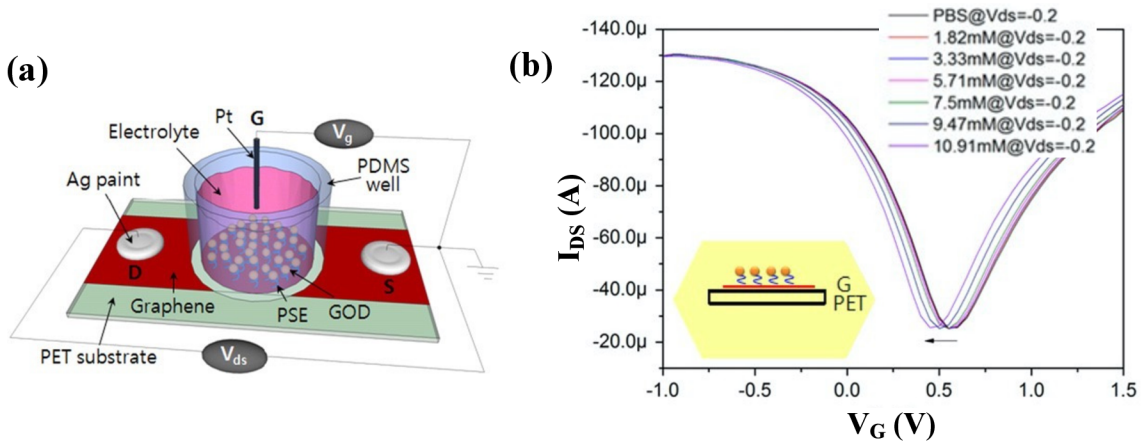

Figure 3.7: (a) The experimental apparatus of the solution gated GFET sensor based on GOx immobilized *via* linker molecule PSE. (b) Charge transfer curves in response to the glucose concentrations, which corresponds to graphene n-doping. The Dirac point shifts towards lower V_G for higher glucose concentration. Taken from [19].

bent substrate exhibited an improved signal thanks to the extended effective reaction area of the channel.

In addition, the authors also examined the response to a gradual increase in glucose concentration (i.e. real-time measurement), showing that the GFET-based sensor met adequate resolution as well as continuity.

As mentioned above, the silk fibroin-encapsulated GFET biosensor from Ref. [17] utilizing CVD graphene was developed for glucose detection. To maintain the same active area for detection, a thin PDMS film with drilled holes was used on the GOx/silk film. The drain and source electrodes were fabricated from Au layer adhesively attached to a subjacent layer of Ti, the solution-gate electrode was connected through a second shadow patterned mask.

The charge transfer curves of the device (shown in Fig. 3.2e) demonstrate the change of channel's conductance in a response to different glucose concentrations. For a fixed value $V_{DS} = 0.1\,V$ and increasing glucose concentration, the Dirac point shifts toward higher V_G, indicating the p-doping effect. The measurable range of glucose concentration of the sensor was reported to be from 0 to 13 mM, with a linear response dependence between 0.1-10 mM. The authors further tested the continuous response of the sensor upon increasing glucose concentration, as well as to the substances that often adversely affect glucose detection (Fig. 3.4a). For common interferences such as uric acid, ascorbic acid, or bovine serum albumin, and the sensor did not show any response (i.e. no change in sensor's conductance). The sensor was able to recognize glucose at a concentration of only 0.1 mM, moreover, high selectivity was confirmed. Additionally, the time series measurement shown in Fig. 3.4b proved that the sensor responded continuously to the fluctuation of glucose concentration in less than 10 sec.

4. Fabrication of the sensor

The experimental part is focused on the design and fabrication of the selective graphene-based biosensor, including measurements of its transport responses to specific analytes. Graphene represents the transducer element in the biosensor. To engineer specificity in such a device, it is necessary to functionalize the graphene surface with molecules able to specifically recognize the detected molecules. Glucose solutions of various concentrations were chosen as the detected analyte, and the selectivity of the sensor was achieved by employing glucose oxidase as the recognition element. The specificity constant of GOx for glucose, which represents how efficiently an enzyme converts a specific substrate into products, is at least 30 times higher than for other sugars [90]. The immobilization of GOx on the graphene surface is achieved by the functionalization process itself using a PSE linker molecule. An essential part of the experiment was the confirmation and characterization of the functionalization, which was performed using Raman spectroscopy and atomic force microscopy.

4.1 Sensor description

Figure 4.1a illustrates the diagram of the fundamental sample utilized for the biosensor. The biosensor is based on a 525 µm thick silicon substrate, a 285 nm thick SiO_2 layer, CVD-grown graphene, and Au electrodes. In the biosensor devices, the Si-based substrate is a suitable choice thanks to a low-cost and mature technology, fundamental for mass production and the possibility of integration in a miniaturized electronic devices [91].

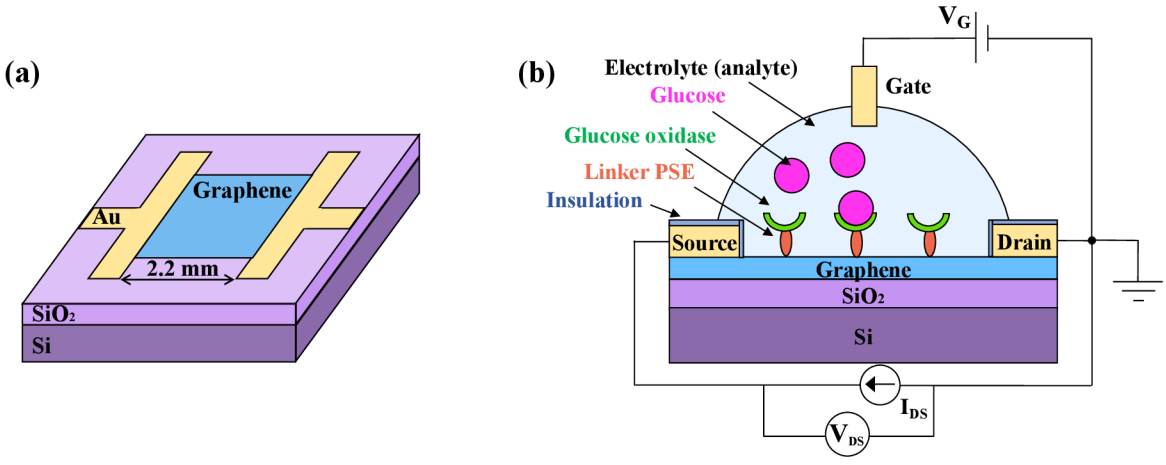

Figure 4.1: (a) A schematic representation of the fundamental sample used in the biosensor. (b) The experimental apparatus of the solution-gated biosensor device. The graphene channel is functionalized with PSE linker molecules and immobilized glucose oxidase which reacts with glucose in the solution.

CVD-grown graphene on copper foil is first spin-coated with a thin layer of PMMA. Then, the PMMA/graphene/Cu film is immersed in $Fe(NO_3)_3$ solution until the Cu is

completely etched away. The released PMMA/graphene film is washed by DI water and transferred onto a SiO_2/Si substrate with gold electrodes spaced 2 mm apart made by electron beam lithography. Finally, the PMMA layer is removed by acetone, IPA and ethanol, and Au electrodes are used as a contacting area for wires connected to an electrical circuit. However, water molecules are trapped between the graphene and the substrate layer due to the transfer process or long exposure to ambient conditions. The interfacial water causes graphene to tear when dripping or washing graphene with aqueous solutions. In order to prevent the tearing, the samples were annealed at 170 °C for 30 minutes to remove the water.

4.2 Biological and chemical materials

Phosphate buffered saline 10**xPBS** of pH 7.4 was purchased from Lonza and diluted serves as a stock solution for glucose oxidase and glucose. 1xPBS buffer with ionic strength 162.7 mM was utilized to stock glucose oxidase to emulate physiological environment. The ionic strength is directly proportional to the concentration of ionized species. The term is used to express the effect of ions in solution on the electrostatic potential [92]. To obtain 10 mL of 1xPBS, 1 mL of 10xPBS buffer KH_2PO_4.NaCl.Na_2HPO4 was diluted in 9 mL of DI water.

1**-Pyrenebutanoic acid succinimidyl ester** linker molecules (dry powder) and the solvent **dimethylformamide**, both purchased from Sigma-Aldrich were used in the form of 5 mM solution for the first step of the graphene functionalization.

Glucose oxidase enzyme (lyophilized powder) purchased from Sigma-Aldrich, was prepared at a concentration of 10 mg/mL in phosphate buffer.

D-(+)-glucose (anhydrous powder) purchased from Sigma-Aldrich was utilized for the preparation of glucose solutions. A set of solutions with different values of glucose concentration in PBS was used for the measurement. The molar concentration or also the substance concentration expresses the substance amount of a substance dissolved in a unit volume of solvent by the equation:

$$c = \frac{n}{V} = \frac{m}{MV} \quad \text{(mol/L, M)}, \tag{4.1}$$

where n is the amount of the solute in moles, V is the volume of the solution, m is the mass of the solute, and M is the molar mass of the solute.

To give an example, for 1 mL of 1 mM glucose solution, 1 mL·1 mM·180 g/mol = 0.18 mg of glucose is diluted in 1 mL of the PBS buffer (from Eq. 4.1). Similarly, for a 5 mM linker solution, 2 mg of PSE in 1 mL of DMF was mixed, where the molar mass of PSE is 385 g/mol.

4.3 Functionalization of graphene with PSE and GOx

Since the non-covalent functionalization approach is the least disruptive of the surface orbital structure of graphene, it is the best choice in situations when one wishes to best retain the electronic properties of pristine graphene. This is achieved by the non-covalent attachment of a bifunctional PSE linker to the graphene surface. The PSE

then serves as a support for the subsequent binding of the enzyme glucose oxidase.

Parts of the functionalization aspects are shown in Fig. 4.2. The fundamental samples comprised of Si/SiO_2 substrate, graphene, and Au electrodes were incubated in 5 mM PSE solution in DMF at room temperature for 2 hours to attach PSE on graphene. Then, the GFET device was washed with IPA and DI water, sequentially, to remove adsorbed linker molecules and to make the surface free from solvents. After that, 10 mg/mL GOx in 1xPBS was introduced to the sample in the refrigerator overnight to attach onto PSE molecules. PSE is a bifunctional linker that contains a pyrene group that stacks with graphene by $\pi - \pi$ stacking, and an N-hydroxysuccinimide (NHS) ester that reacts with primary amines of protein, or enzymes [31]. Finally, the sample rinsed with a 1xPBS buffer to remove excess unreacted GOx, and furthermore rinsed with DI water to clean the salts from the graphene surface.

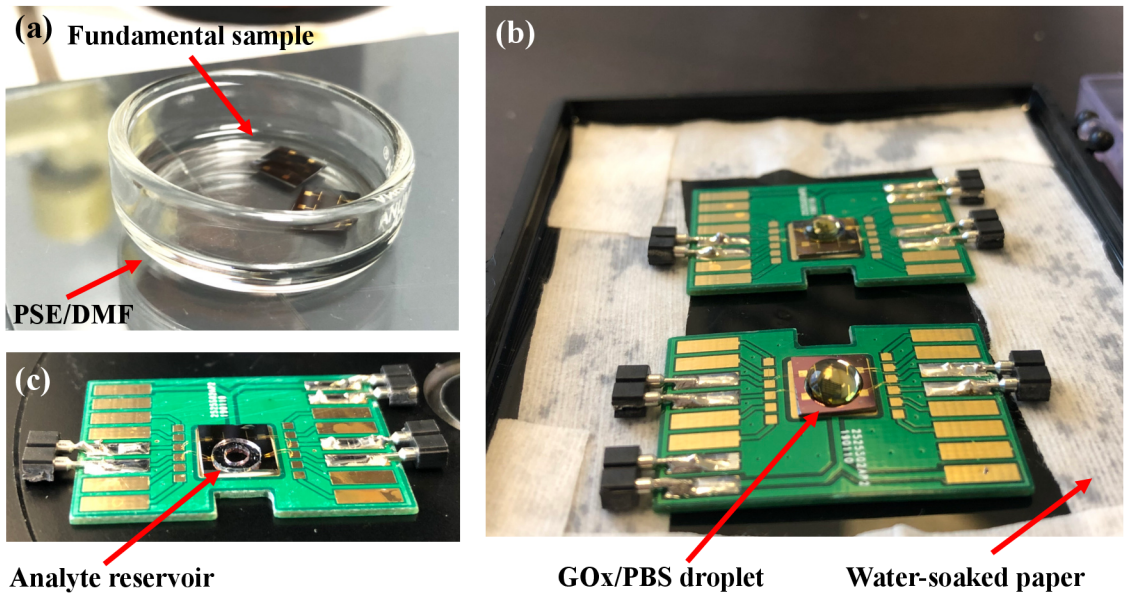

Figure 4.2: The functionalization procedure. (a) The sample immersed in PSE/DMF at RT, to bind the PSE linker to the graphene surface. (b) The sample glued to an integrated circuit to facilitate the handling of the electrical measurements for the device. The GOx/PBS droplet on the surface of the sample during the subsequent immobilization of GOx. (c) Following the functionalization, a silicon reservoir is placed on the graphene channel to facilitate the operation and to maintain the same active area.

4.4 Challenges during the functionalization

There were several challenges in manufacturing the sensor. The functionalization process itself is time and material consuming. DMF is a strong organic solvent that penetrates commonly used resists, gels or plastics which are utilized to define areas of graphene and makes them swell. Owing to its polar aprotic characteristics [93], DMF also dissolves most adhesives, tapes or organic compounds, thus when rinsing, DMF contaminates graphene surface with impurities. Therefore, it is not possible to place everything in the sensor arrangement first, including defining the detection area,

and electrical contacting, and then perform the first functionalization step to bind the PSE molecules. Although the evaporation rate of DMF is low, it is also inappropriate to functionalize graphene with a drop of PSE/DMF on the surface due to the mentioned contamination during rinsing. In addition, the DMF droplet shows a spontaneous spreading and spills over the entire surface. This is because DMF exhibits high wettability compared to water [94]. In the first functionalization step, it is more advantageous to immerse the whole fundamental sample in the solution (as seen in Fig. 4.2a). It was later proved by AFM analysis, that samples immersed in PSE/DMF bound the PSE molecules more strongly and homogenously than samples dripped by this solution. After that, the sample is glued to the expander and connected to the electrical circuit.

In contrast, the wettability of PBS is similar to that of water which allows performing GOx functionalization by simply dripping a sample with GOx/PBS solution. Later, testing of the sensors revealed that it was convenient for the buffer to be refrigerated for the mixing with GOx. Binding of GOx takes from 10 to 16 hours, during which time the aqueous PBS solution can evaporate significantly. To prevent the evaporation of the solution from the sample surface, it must be placed in saturated water vapors. This was accomplished by placing the sample on soaked dust-free paper enclosed in a Petri dish. Moreover, it is necessary to monitor the temperature and time when handling GOx. The lyophilized enzyme is stored at $-15\,^{\circ}\mathrm{C}$ and stored in a refrigerator after mixing with PBS. The enzyme mixed with PBS gradually loses its activity, therefore it is necessary to prepare it fresh before each functionalization and perform the measurement as quickly as possible.

5. Characterization of the functionalization process

Raman spectroscopy was applied for the structural analysis of the deposited graphene, in particular to confirm the presence of monolayer graphene and the non-covalent functionalization on graphene surface. AFM was used to characterize the surface morphology of graphene upon individual functionalization steps.

5.1 Characterization by Raman spectroscopy

To verify the nature of binding between PSE molecules and graphene, Raman spectroscopy measurements were carried out before and after treatment with PSE. The measurement was performed under room temperature on an NTEGRA Spectra instrument from the manufacturer NT-MDT. The laser excitation 532 nm was used and the power was set below 1 mW to avoid the sample heating. In order to minimize the errors due to the variations in graphene samples, the data were taken in 4 different points of sample and averaged. The Raman spectra are shown in Fig. 5.1a,b, where the blue curve represents the Raman spectrum of untreated graphene, the red curve represents PSE functionalized graphene.

The most important characteristics in Raman spectra of single-layer graphene are G peak lying at 1582 cm^{-1} (representing graphite) and 2D peak, lying at 2700 cm^{-1}. The G peak belongs to the double degenerate phonon mode in the middle of the Brillouin zone. It is the only one visible in first-order Raman scattering and is mainly based on sp2 orbitals. In the absence of defects, the intensity of the 2D peak is greater than the G peak, and with increasing number of defects or greater graphene doping, this differences decreases. The disordered D peak at 1350 cm^{-1} is not obvious until defects exist in graphene samples [95].

After the PSE functionalization, in the region around the G band, several peaks related to PSE appear. These characteristics can be seen in the broader spectrum of Fig. 5.1b. A slight increase in the intensity of the D peak at 1350 cm^{-1} was observed and is attributed to the sp^3 orbital hybridization of the PSE molecule with graphene plane [61, 96]. This suggests the PSE functionalization did not significantly alter the doping level and causes minimal disorder in the graphene [97]. Other characteristic peaks of the corresponding PSE molecule were observed at 1241 cm^{-1}, 1394 cm^{-1}, and 1436 cm^{-1}, and are consistent with the Raman spectra of PSE from previous studies [52, 98, 99]. The D' peak located around 1623 cm^{-1} is obvious, as shown in detail in Fig. 5.1c, and is attributed to pyrene group resonance [58, 96, 62, 100]. The intensity ratio of the G peak and its shoulder D' peak after functionalization, $I(G)/I(D')$, is between $8-9$. Moreover, the presence of PSE is further supported by the background of the spectra caused by fluorescence emission of the PSE known as a fluorescent dye, as shown in the fluorescent background of spectrum Fig. 5.1b. It is worth mentioning that the Raman spectra were taken after the sample had been rinsed and dried, further

confirming the attachment of the PSE linker to graphene. For comparison, Fig. S8.1 in Chapter 8 - Supplementary material contains previously published Raman spectra of PSE functionalized graphene.

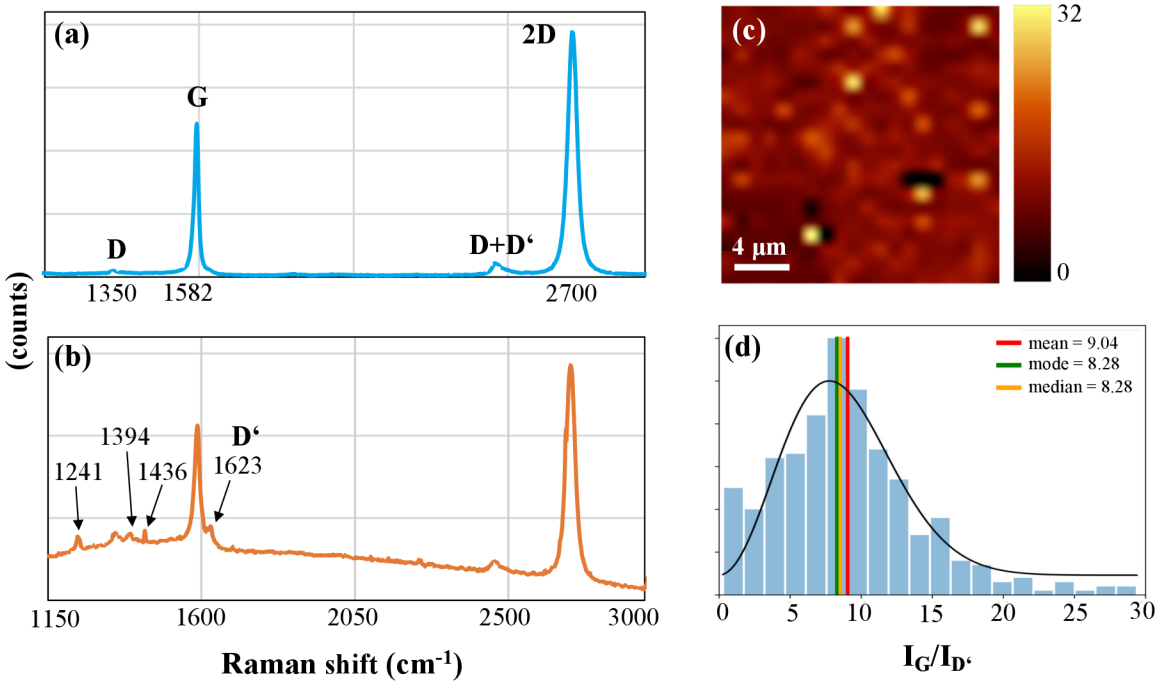

Figure 5.1: Raman spectra of (a) graphene and (b) graphene functionalized with PSE in DMF. Raman G peak for (c) The distribution of the intesity ratio $I(G)/(D')$ of PSE functionalized graphene and (d) the corresponding G/D' Raman intensity ratio map.

5.2 Characterization by atomic force microscopy

Atomic force microscopy imaging was performed to measure the change of the graphene topography during the functialization process. The method provides a quantitative information about the shape of the enzyme GOx adsorbed on the sample. The topographical images were collected using Bruker Dimension Icon in tapping mode (with ScanAsyst auto-optimization of gain, setpoint and scan rate).

All the functionalization steps are shown in AFM images of graphene flakes in Fig. 5.2. After the first step (Fig. 5.2b), no significant modification of the graphene surface can be seen, indicating that the PSE coverage is uniform. After immobilization of GOx (Fig. 5.2c), a noticeable modification of graphene flakes appear. Major portion of the graphene surface is covered with the enzyme molecules. Individual GOx monomers or dimers are barely distinguishable, as their lateral dimensions are approximately 6.5 x 5 nm and 10 x 6 nm, respectively [101]. The visible globules of lateral dimensions of tens of nanometers correspond to clusters composed of multiple molecules commonly occuring at high enzyme concentration [101].

Topographic data were analysed to determine the thickness of graphene, the PSE layer and the GOx layer. Fig. 5.3 shows height profiles taken from AFM line scans of untreated graphene, PSE functionalized graphene, and graphene functionalized with

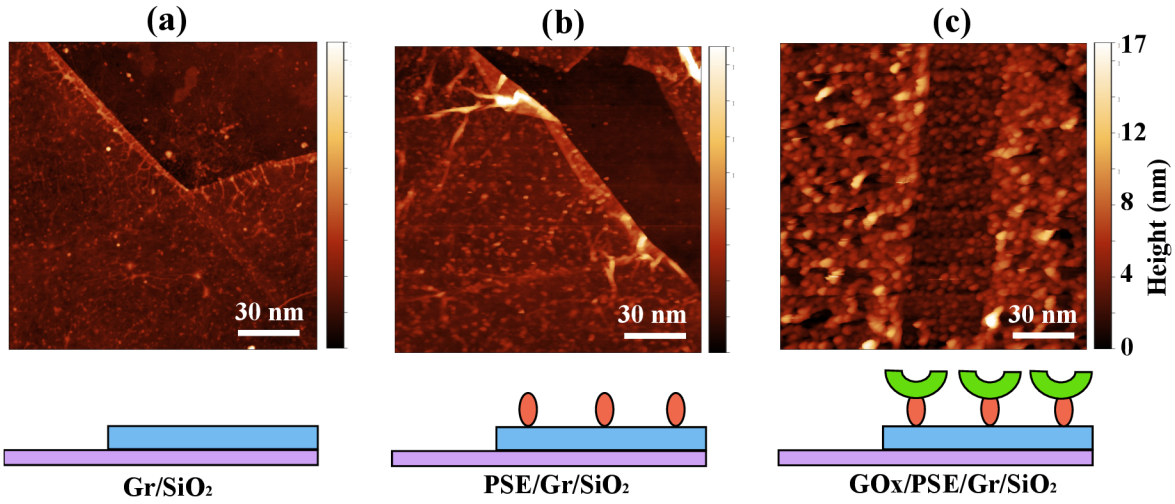

Figure 5.2: AFM images of the functionalization procedures: (a) untreated graphene, (b) PSE functionalized graphene, and (c) graphene functionalized with PSE and immobilized GOx. The sample was introduced to PSE in DMF for 2 hours, and to GOx in PBS for 16 hours. The scanning area is 1.5 µm.

PSE and immobilized GOx molecules. In order to minimize the errors due to the variations in height profiles, data from 10 line scans were averaged over two AFM images of scanning areas of different size. Significant height alternations due to graphene layering or impurities were not included in the averaging.

The line scans show the height of CVD-grown graphene ∼1 nm (Fig. 5.3a), which can be attributed to the presence of the graphene monolayer. The first functionalization step resulted in an uniform, ∼0.8 nm thick layer of self-assembled PSE on the graphene surface (Fig. 5.3b), which is in agreement with results published in Ref. [62, 102].

The line scans confirmed the immobilization of the GOx molecules (Fig. 5.3c). The line scans taken from 1.5 x 1.5 µm scanning area, elevation profiles were read in areas of uniform coverage that are more prevalent. These regions show an average increase of about 4 nm in height, which corresponds to a single layer of GOx molecules immobilized on the surface. In case of line scans taken from 9 x 9 µm scanning area, the average layer height was ∼1 nm higher than for the smaller scanning area. This confirms the presence of three-dimensional clusters in which at least two layers of molecules are present. The concentration of three-dimensional clusters is lower than that of single-layered clusters, as can be seen in AFM image (Fig. 5.2c), and is in an agreement with results reported in Ref. [101].

Nevertheless, it must be pointed out, that the GOx enzyme molecules are also present on SiO_2. The enzyme coverage does not show significant height contrasts indicating the presence of large clusters. Such results suggest that the molecules are immobilized on SiO_2 by physisorption, because the covalently bound molecules tend to form larger clusters with a slightly lower concentration on the surface, as reported in Ref. [101, 103].

Furthermore, the procedure for GOx immobilization was tested for a shorter time (10.5 h) and at a slightly lower concentration of GOx in PBS. Similar features were

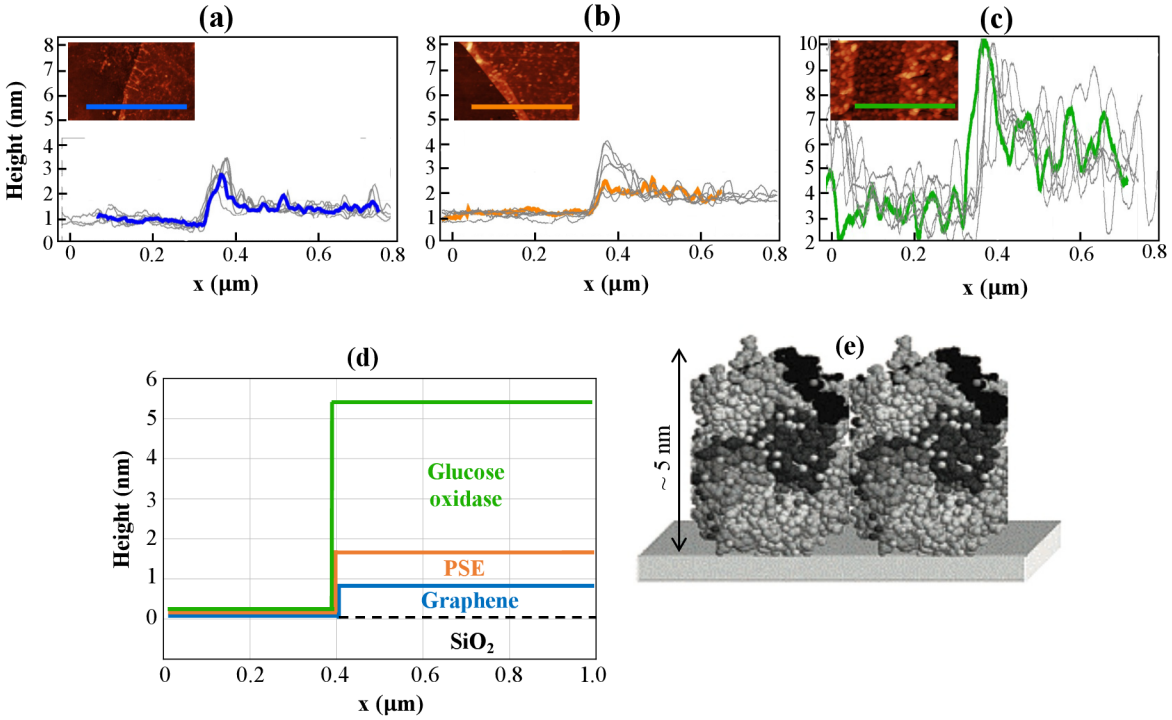

Figure 5.3: AFM line scans of (a) untreated graphene, (b) PSE functionalized graphene, and (c) graphene functionalized with PSE and immobilized GOx. The gray curves represent 0.8 µm line scans derived from AFM images in Fig. 5.2 used for the statistical evaluation. The colored curves are shown as a representative plot and illustrated in the inset figures. (d) Comparison of average height profiles for each step of the procedure. (e) A model of the GOx molecule on the surface in a lying position, taken from [101].

observed in various AFM images, shown in Fig. 5.4a,b. As in the case of the images in Fig. 5.2, GOx molecules are adsorbed on the SiO_2 surface. However, black holes of tens of nanometers in diameter are visible in the GOx layer on the graphene surface. Such results correspond to an arrangement, in which a few GOx molecules are linked to each other on the surface in a tight cluster with a hole in the center, as published in Ref. [101], and illustrated in Scanning tunneling microscopy (STM) image in Fig. 5.4c,d.

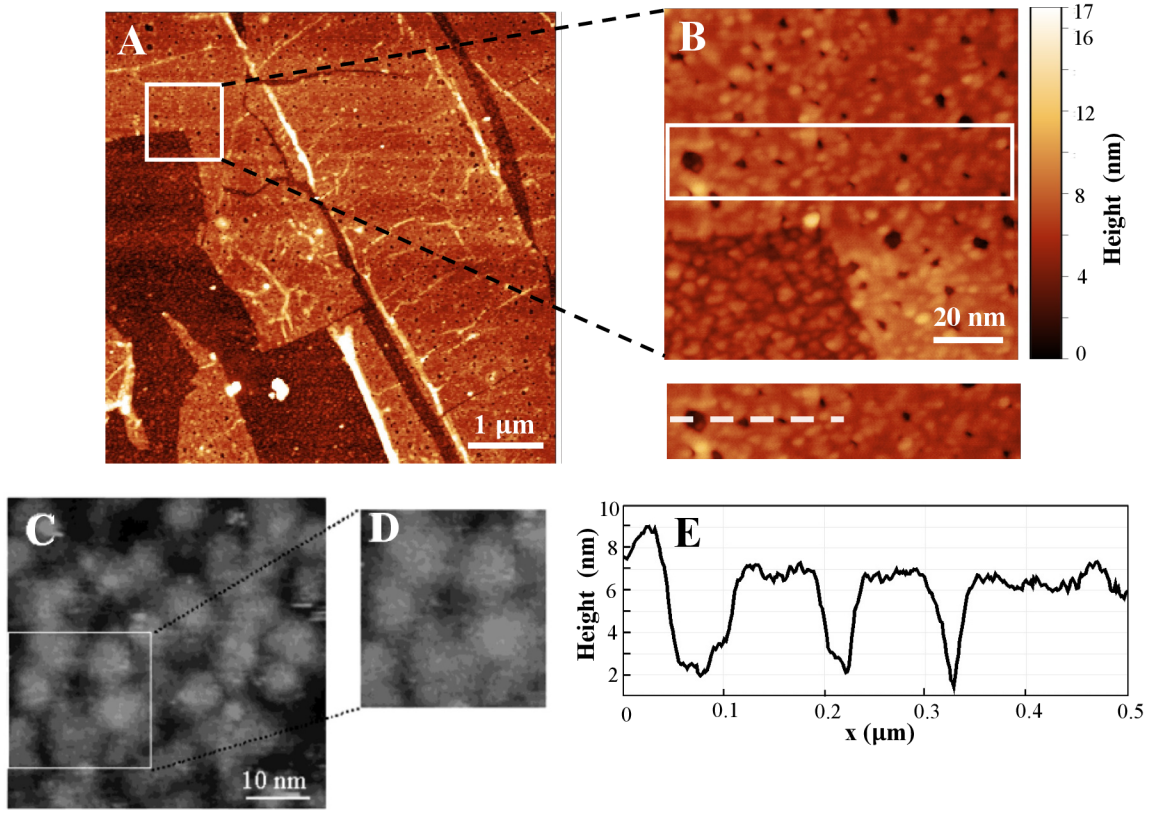

Figure 5.4: AFM images of graphene functionalized with PSE and immobilized GOx: (a) size 6 x 6 µm, (b) size 1 x 1 µm. The sample was introduced to PSE in DMF for 2 hours, and to GOx in PBS for 10.5 hours. (c) STM image of a GOx monolayer adsorbed on the surface size 100 x 100 nm, and (d) zoom of (c), both taken from Ref. [101]. (e) The line scan represented by the dashed white line in AFM image (b).

6. Electrical characterization

After confirming the functionalization of graphene, the electrical measurements were performed. First, the transfer characteristics in the GFET arrangement were measured to determine graphene doping. The order of the individual electrolyte concentrations given in the legends always corresponds to the order in which the experimental measurement itself was performed. Furthermore, the real-time sensor responses were investigated. Measurement parameters setting and data acquisition were controlled *via* LabVIEW designed program [104].

In order to preclude the GOx molecules from degradation, the functionalized graphene channel was prevented from being exposed to air during the measurement. When the concentration of the glucose solution was varied, a certain volume of electrolyte was first removed and then the same volume was added. The resulting concentration was then recalculated.

Optimizing buffer

As mentioned above, in solution-gated FET devices, the electrical-double layer formed between electrolyte and graphene acts as an insulator. The thickness of the insulating layer is known as the Debye length and depends on the ionic strength of the electrolyte. In high ionic strength electrolytes, the Debye length is shorter than in those with lower ionic strength [72]. In GFET biosensors, the interaction between detected molecules and bio-receptor molecules immobilized on the conductive channel must occur within the Debye length [100]. Otherwise, the channel faces a severe charge screening effect. In order to effectively detect glucose molecules with GOx functionalized graphene channel, the buffer solution has to be diluted to reach a larger Debye length. For an aqueous solution at RT, this length becomes $\lambda_D(\text{nm}) = 0.304/\sqrt{I}$ where I is the ionic strength in mol/L [70]. The Debye length of highly ionic 1xPBS is around 0.7 nm [100], which is much smaller than the measured PSE/GOx layer of $4-10$ nm (Fig. 5.3). Therefore, the detection measurements of glucose were carried out in 0.01xPBS with ionic strength 1.627 mM and gives λ_D of approximately 7.6 nm, which is therefore large enough to contain the point of interaction between GOx and glucose molecules. 10 mL of the buffer was prepared by diluting 0.1 mL of 1xPBS in 9.9 mL of DI water.

Sensor details

The electrical measurements in this chapter were performed on a sensor consisting of graphene flake (4 x 4 mm) on a Si/SiO_2 substrate forming the fundamental sample. To improve the stability of graphene to liquids and cleaning, the fundamental sample was annealed for 30 minutes at 160 °C in atmospheric conditions. The sample was then immersed for 2.25 h in 5 mM PSE/DMF to attach the linker molecules. Subsequently, the sample was alternately rinsed twice with water and twice with IPA. The edges of the sample were insulated with Kapton tape to prevent charge leakage through the substrate. The graphene was contacted with silver conductive paste and connected

to an electrical circuit by wires. A GELPAK® film reservoir for the analyte of about 4 mm^2 was formed on top of the sample. A drop of GOx/1xPBS mixed just before dripping was placed in this reservoir. The sample was put into the refrigerator for 15 hours. Finally, it was rinsed several times with 1xPBS to wash away the unbound enzyme and intensely with water to wash away the salts from the buffer. In the production of this sensor, the smallest possible time delay between the individual steps was achieved. The electrical measurements took place immediately after the GOx functionalization. The sensor in the GFET measuring arrangement with the solution gate is illustrated in Fig. 4.1b.

6.1 Charge transfer curves

In the proposed solution-gate FET, the conductance of the graphene channel is modulated by the gate voltage. To measure the transfer characteristics of the solution-gate GFET, a lock-in amplifier Standford Research SR830 with the resistor 10 MΩ in series was employed. Such resistance is much higher compared to the resistance of the sample, thus low current flow through the sample is maintained and the channel is prevented from damaging. The signal amplitude was set to 1 V, time constant 100 ms, and frequency 1333 Hz. The gate voltage was applied by immersing a tungsten wire electrode into the PBS analyte on top of the GFET device. Figure 4.1b illustrates a diagram of the GFET-based glucose biosensor. The conductance of the graphene channel changed with the applied solution gate. The outcome of this measurement is the transfer curve, i.e. the device resistance (R_{DS} vs. V_{G}) curve (as represented in Fig. 3.2). The point of maximum resistance on this curve is called the Dirac point and its position describes the doping of graphene.

Glucose solutions were prepared by mixing dry glucose in 0.01xPBS buffer. To determine the doping effect introduced by the PBS, 12 µL of the buffer was first added to the graphene channel and transfer curves were measured. The Dirac point stabilized at −0.29 V and no further shift was observed even after 6 minutes. This value served as a reference value for pure PBS and suggests that PBS n-dopes the functionalized graphene channel. Glucose concentrations in the transfer curves follow the established color convention, blue corresponds to PBS, pink to 5 mM, green to 7 − 8 mM, red to 10 mM, and orange to values above 20 mM.

Transfer curves were measured for glucose concentrations of 5 mM, 8 mM, 0 mM (PBS), 21 mM, respectively (Fig. 6.1). A positive shift of the Dirac point was observed when glucose solution was introduced to the channel and cause p-doping respective to initial doping introduced by PBS. For 5 mM the Dirac point was shifted to $V_{\mathrm{G}} = -0.25$ V and after a further increase to 8 mM, it shifted slightly another 0.01 V to the right. Then the electrolyte was intensively diluted with PBS and the DP stabilized at −0.29 V which indicates, that it contained insignificant amount of glucose. During the dilution, the electrolyte volume was still maintained at ∼ 12 µL. Next, glucose was added to the channel resulting in 21 mM and the DP moved towards positive values. After 6 minutes, the DP position has moved 0.03 V from −0.26 V to −0.23 V, exhibiting a slightly delayed response. All measurements indicating the positive shift of the Dirac point correspond to graphene p-doping (removing electrons) by glucose

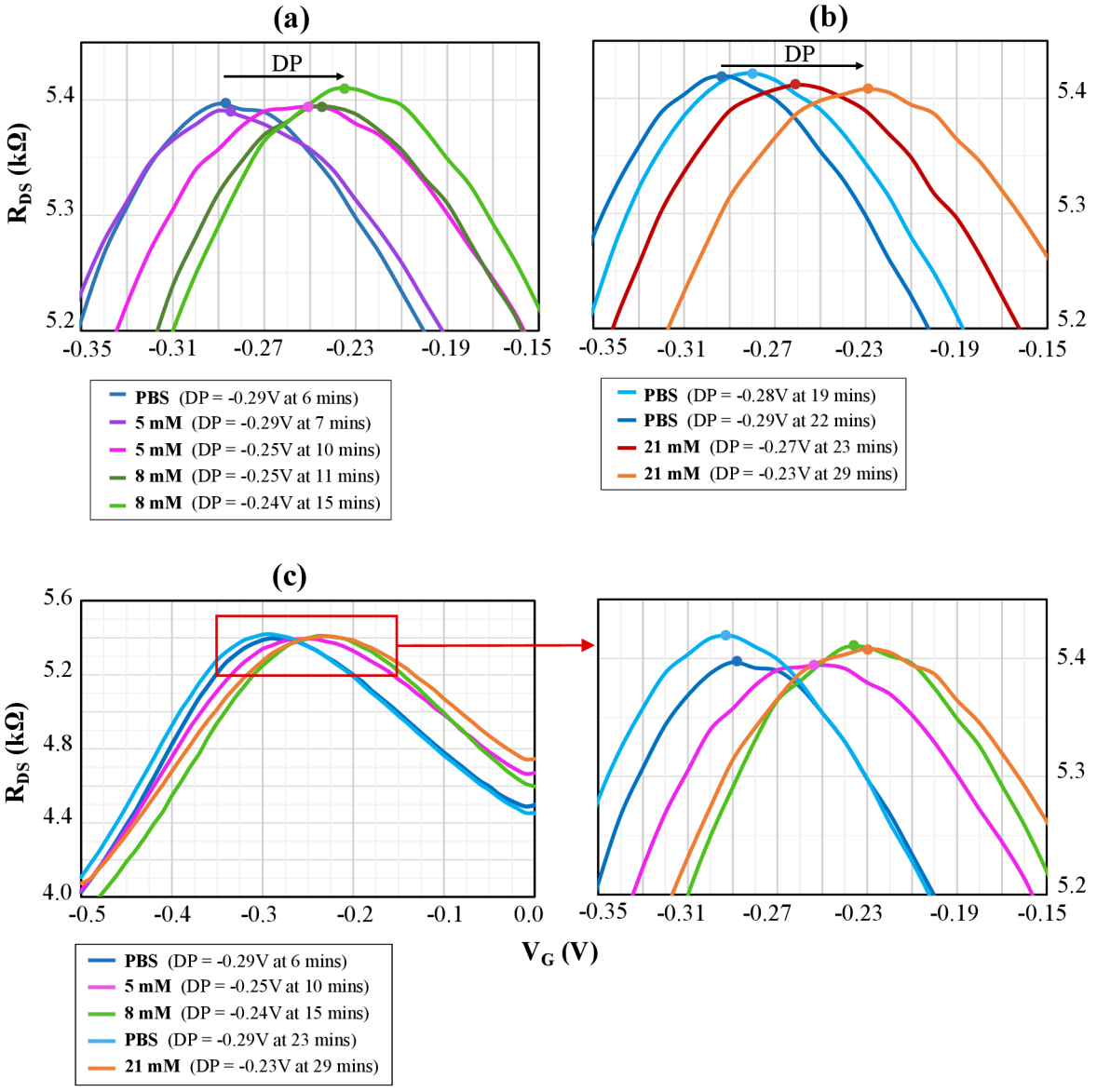

Figure 6.1: Transfer curve of the GFET sensor in response to the addition of various glucose concentrations in the range of $0 - 21\,\text{mM}$. The circles indicate the position of the Dirac point. For all glucose concentrations, the positive shift of DP from the PBS position occurs when glucose is present. First, PBS was added to the channel at 0 minutes and let for 6 minutes. (a) and (b) contain the curves measured immediately after the change in concentration and then after a few minutes. (c) Representative curves for individual concentrations after stabilization selected from (a) and (b).

concentration increase. The electrolyte was then diluted from 21 mM to 15 mM, and real-time measurements of the channel resistance took place.

6.2 Real-time response measurements

The resistance measurements of the graphene channel were performed using Keithley 6221 AC/DC Current Source and Keithley 2182 Nanovoltmeter. The resistance was calculated from a voltage difference read by Keithley 2182 Nanovoltmeter. A resistor with 1 kΩ was applied across the drain and source terminal electrodes.

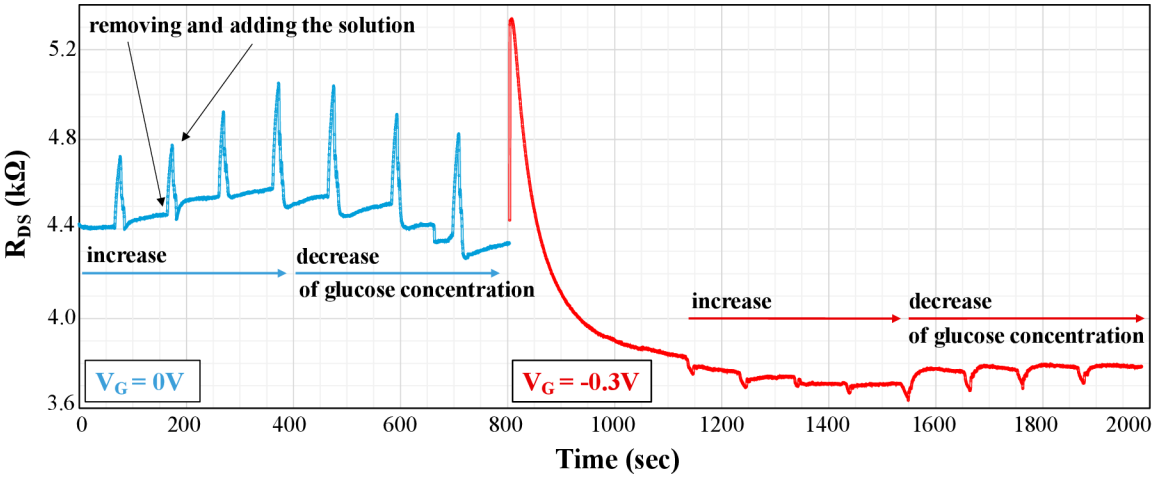

Figure 6.2: Overview of the real-time measurement. At 800 seconds, the gate potential was changed from 0 V to −0.3 V, such that both p- and n-type doping of the graphene channel in FET investigated.

The resistance of the graphene channel changed upon the interaction of glucose with GOx immobilized on the graphene surface. At 0 seconds, the glucose concentration was kept at 15 mM, and the concentration was changed every 100 second. The peaks in the sensor response correspond to removing and adding the same volume of the electrolyte. The first 800 seconds were measured in the n-type region at a gate voltage 0 V (blue curve in Fig. 6.2). Previous results from the transfer curves in Fig. 6.1 shown that in the presence of glucose, the Dirac point is located to the right of $V_G = -0.29$ V. Therefore, the gate voltage was switched to -0.3 V, and the measurements were performed in the p-type region close to the Dirac point (red curve in Fig. 6.2). Details of curves for each region are shown in Fig. 6.3.

In the n-type region of GFET ($V_G = 0$ V, blue curve in Fig. 6.3), as the glucose concentration increases, the resistance of the graphene channel increases. This confirms the results from the transfer characteristics and the presence of glucose cause p-doping of graphene. A slight response of the sensor was observed above the concentration of ∼35 mM. Therefore, at 350 seconds, the glucose concentration was gradually reduced. Finally, the concentration of 7 mM was reached at 700 seconds. The resistance of the channel returned to a lower value than the initial 15 mM, indicating that the sensor response is reversible.

The concentration 7 mM was kept and at 800 seconds, the gate voltage was switched to a value corresponding to the p-type region of GFET ($V_G = -0.3$ V, a red curve in Fig. 6.3). As the glucose concentration increases, the resistance of the graphene channel decreases, confirming again that p-doping occurs in the presence of glucose molecules. Initially, as the concentration increased to ∼ 30 mM, the shape of the curve was affected by the hysteresis caused by the stabilization of the sensor after switching the gate voltage. Nevertheless, the individual steps of the resistance decrease after the addition of glucose are visible. At 1550 seconds, the glucose concentration was gradually reduced and the channel response underwent an opposite trend. From 1900

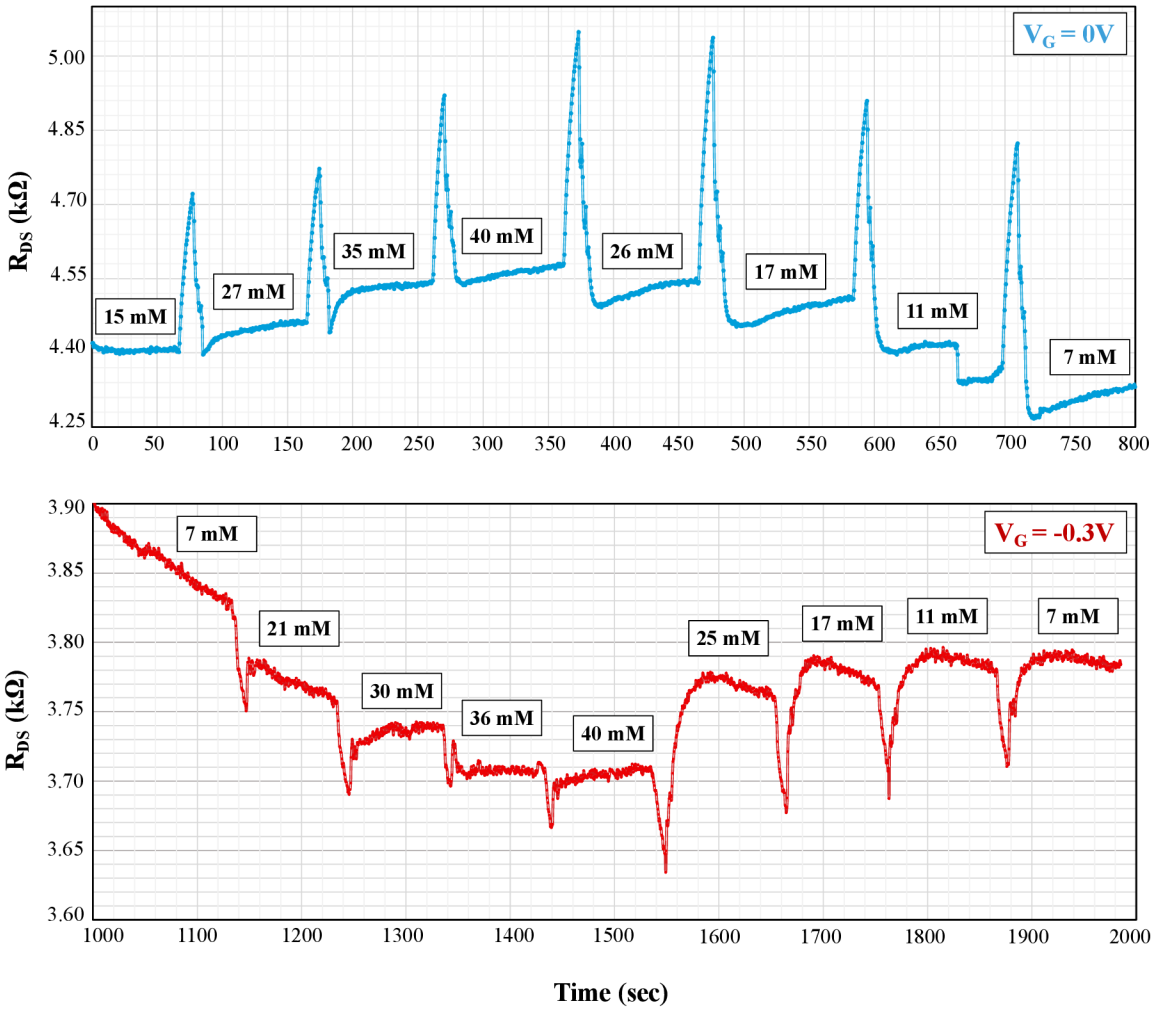

Figure 6.3: Detail of real-time response measurement for gate voltages $V_G = 0\,V > V_{DP}$ and $V_G = -0.3\,V < V_{DP}$ selected to the right and left of Dirac point. In both cases, the glucose concentration was first increased and then decreased.

seconds, the sensor was set to stabilize at 7 mM.

6.3 Further electrical measurements

Subsequently, the transfer curves were measured at 7 mM. The Dirac point was significantly shifted up to $V_G = -0.20\,V$ (Fig. 6.4). The position of the DP was shifted more towards positive values than for the concentration of 21 mM previously measured in Fig. 6.1. This can be attributed to the fact that the reaction of the GOx enzyme is delayed and after intensive measurements up to 40 mM, the accumulated glucose residues still react with GOx. However, within 6 minutes the DP tends to gradually stabilize at a lower value.

The electrolyte was diluted to 5 mM and the sensor's response in real-time was monitored for $V_G = -0.1\,V$ (Fig. 6.5). This voltage corresponds to the n-type region, and as expected, the resistance increased for higher glucose concentrations. Nevertheless, the sensor started to react with a delay and inadequately. For example, when the concentration was initially increased to 16 mM, the resistance decreased, which was

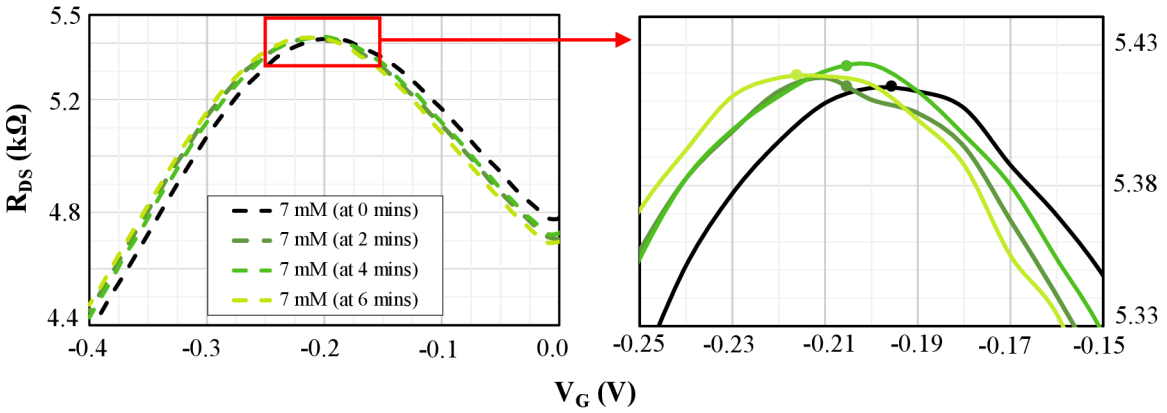

Figure 6.4: Transfer curves for 7 mM performed after the real-time measurements.

attributed to its delayed response on 5 mM. The continuous measurement was terminated shortly after dilution to 8 mM, and to verify the delayed response of the sensor, the transfer curve was measured.

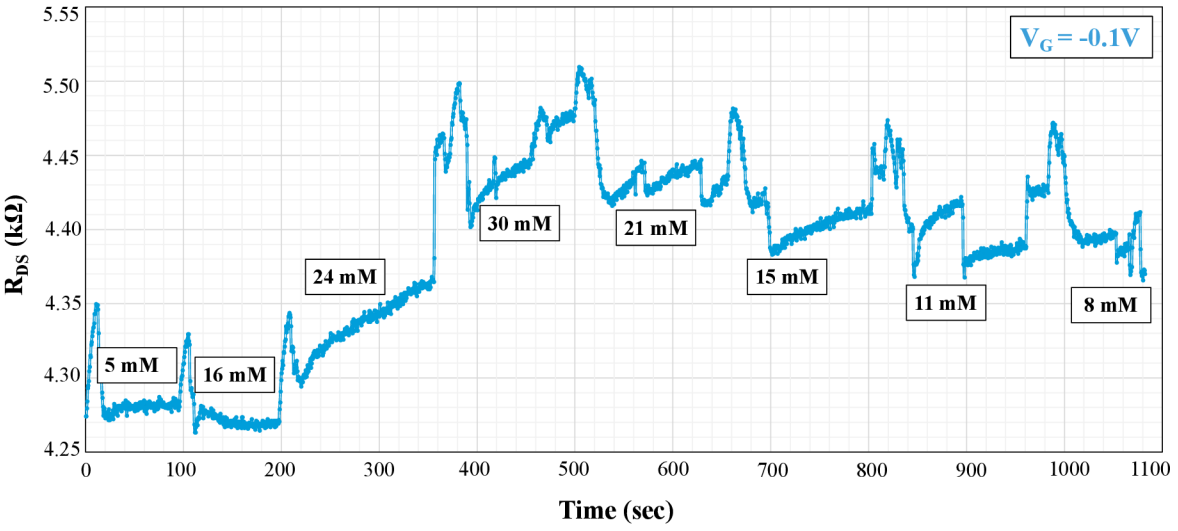

Figure 6.5: Real-time response measurement for the gate voltage −0.1 V corresponding to the n-type region of the FET sensor.

Fig. 6.6 show that after 3 minutes the DP is further shifted 0.03 V to the right from the previously measured value for 8 mM, thus, the enzyme further interacts with glucose. Therefore, the channel was rinsed and supplemented with pure PBS. Within 4 minutes, all accumulated glucose near the graphene channel gradually reacted and the Dirac point shifted from −0.23 V to −0.29 V corresponding to the clear buffer. By adding glucose resulting in 10 mM, the Dirac point shifted slightly by 0.02 V to the right. However, the sensor no longer responded to further increases of concentration. After a few minutes, the Dirac point gradually shifted to the value for the pure buffer (−0.29 V) and stabilized at this value. This can be attributed to the depletion of the activity of the bound GOx enzyme.

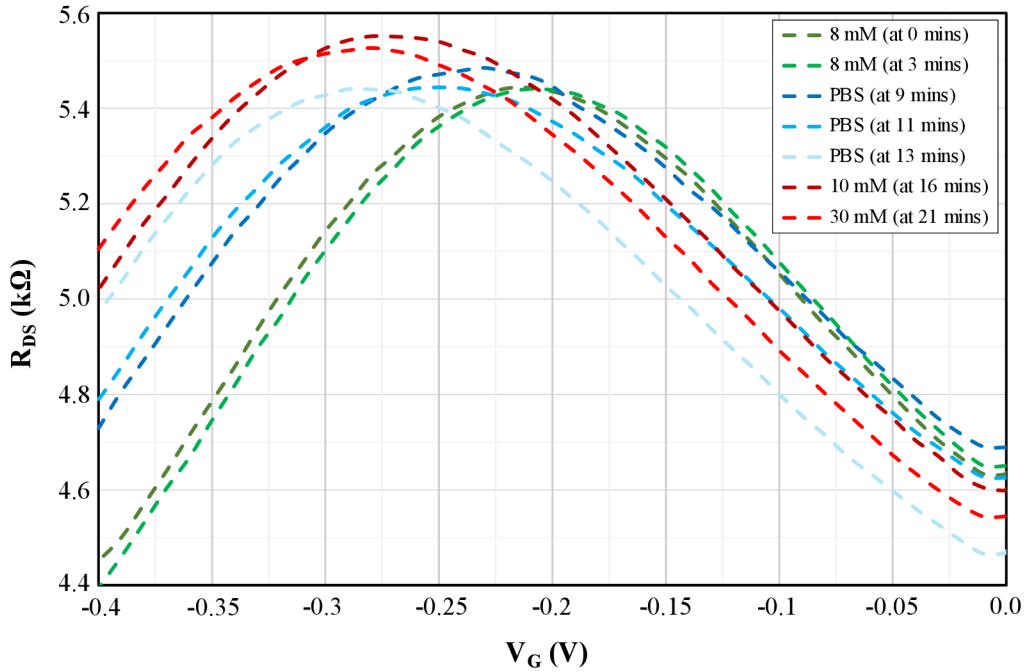

Figure 6.6: Transfer characteristics (R_{DS} vs. V_{G}) of the GFET device when exposed to varying concentration of glucose.

6.4 Results summary

Graphene's electrical properties are modified upon the presence of chemical dopants and adsorbates. In the first functionalization step, the PSE molecules are introduced to graphene and serve as a linker to anchor the enzyme GOx. The doping effects after the surface modification of graphene by the aromatic molecules PSE were investigated in Ref. [53, 61]. It was revealed that PSE molecules have a p-doping effect on the graphene channel employed in GFET.

In the second functionalization step, the GOx molecules are immobilized to the graphene surface through a covalent binding between the succinimidyl ester group of PSE and the amino group of GOx. The doping effect imposed by GOx is considered negligible. GOx is composed of large macromolecules, in which the electroactive site of flavin adenine dinucleotide is deeply buried within the enzyme [105].

However, the type of graphene channel doping can be determined only in the complete setup used for electrical measurement, i.e. including 0.01xPBS serving as the fundamental electrolyte. From the first transfer curves, it was found that graphene is n-doped with a Dirac point at $-0.29\,\mathrm{V}$ in the presence of pure PBS (represented by blue curves in Fig. 6.1, 6.6).

For all glucose concentrations, the p-type doping of the PSE/GOx functionalized graphene channel was observed. However, the same p-doping effect in the presence of glucose for graphene in the FET-based glucose sensor was published in Ref. [17]. The flavin adenine dinucleotide group in GOx catalyzes the oxidation of glucose as summarized in Eq. 1.2 to form gluconic acid and H_2O_2. The H_2O_2 adsorb on the graphene and a series of following reactions illustrated in Fig. 6.7 result in p-type

doping of graphene in the presence of H^+ [17].

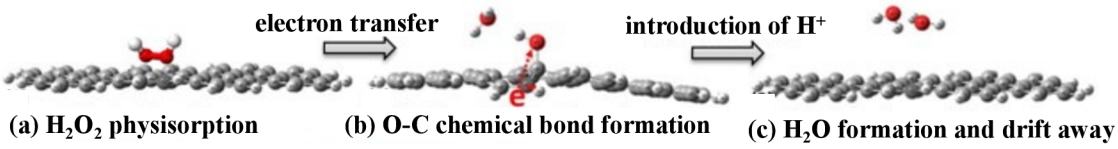

Figure 6.7: Schematic illustrations of p-type doping effect caused by H_2O_2 reduction reaction at graphene surface. (a) H_2O_2 physisorption without the formation of a chemical bond. (b) breakage of the O–O bond in the adsorbed H_2O_2 molecule and formation of one adsorbed OH group and the first H_2O molecule; Electrons transfer from graphene to H_2O_2 cause p-type doping to graphene. (c) Cleavage of the C–O bond between oxygen and graphene and the formation of the second H_2O molecule. H_2O molecules drift away with the electrons obtained from graphene. Gray color represents carbon, red oxygen, white hydrogen. Taken from Ref. [17].

The transfer curves were not extensively tested for the sensor's response to a gradual decrease in concentration. Nevertheless, the first measurements in real-time (Fig. 6.3) show a tendency of the channel resistance returning to the original values as the glucose concentration decreases.

The initial measurement for gate voltage $V_G = 0\,V$ from Fig. 6.3 was chosen as the most verifiable for comparing the sensor response. The evaluation was based on the relative change in resistance $(R - R_0)/R_0$, where R_0 and R are the resistance of graphene channel before and after the change in glucose concentration, respectively (R values were read after 80 seconds). Due to the difficulty of evaluation, the value for 11 mM was not included. In each step, the change in concentration was in the range of $5-14\,mM$, and the change in resistance was about 1 %. As the concentration decreased, the relative change in resistance was lower, which is attributed to the accumulation of glucose around the enzyme molecules. Such changes in resistance are not significant, however, it should be noted that these correspond to tens of Ω and to changes in current I_{DS} in the order of µA units. Similar results have been reported in the literature for the detection of glucose by GOx-functionalized GFET. For example, changing the glucose concentration by 10 mM (from 0 mM) resulted in I_{DS} change of $\sim 4\,\mu A$ in Ref.[60], $\sim 6\,\mu A$ in Ref. [19], and $\sim 14\,\mu A$ in Ref.[17].

During the last transfer curve measurements shown in Fig. 6.6, the enzyme activity was gradually depleted, which may have occurred for several reasons. The detection area ($\sim 4\,mm^2$) in the fabricated sensor was relatively small comparing to that of previously published GFET-based glucose sensors. During the whole measurement, the electrolyte concentration on the graphene channel was changed more than thirty times and the enzyme could also wash away. Furthermore, high concentrations above 35 mM were used, which is more than five times more than in commercial glucometers, since the reference range of medical examination for diabetes is generally made at the glucose level under 7 mM [17].

In order to accurately characterize the response of the sensor to a certain glucose concentration, it is suggested that measurements are performed more elaborately. In this case, to perform only one type of electrical measurement (transfer curve/real-time

response) on the same sensor in order to avoid interference. In addition, it is necessary to evaluate and include the required stabilization time in both measurement setups. To determine the sensitivity, measurements of multiple sensors manufactured in a unified manner are further required.

7. Conclusion

In recent years, intensive research has been focused on the development of graphene-based bioanalytical sensors in FET configuration. In the GFET, graphene is employed as the conductive channel and serves as the sensing platform for the detection. To detect the existence of specific biomolecules in a target sample, a functionalization by recognition molecules to graphene is necessary to be performed. Such GFET-based devices then enable the detection of, e.g. nucleic acids (DNA single-nucleotide polymorphism, DNA and RNA sequences) [31, 98, 106, 107], opioids [108], proteins [96], or viruses such as ebola, pathogenic rotavirus [109], or newly emerging coronavirus SARS-CoV-2 [110, 111, 112].

Based on previous studies, the analytical section of this work contemplates methods of functionalizing pristine graphene. Emphasis is given to fundamental advances of glucose sensing principles and related materials. Building on prior findings, it is shown that the functionalization of graphene with 1-pyrene butanoic acid succinimidyl ester enables a stable linker bridging for the attachment of a functional group. Further, as a result of the surface modification by the PSE linker molecule, the immobilization of an enzyme glucose oxidase on graphene is reported. This covalent attachment of an enzyme glucose oxidase enables the molecular recognition of glucose. The surface modification during GOx immobilization was proved by Raman spectroscopy and Atomic force microscopy.

The Raman spectra of graphene before and after PSE functionalization support that the graphene surface has been non-covalently functionalized with PSE. The disordered D peak lying at $1350\,\mathrm{cm}^{-1}$ mildly increased, and the D' peak attributed to the pyrene group of PSE appeared at $1623\,\mathrm{cm}^{-1}$. Emergence of several peaks ($1241\,\mathrm{cm}^{-1}$, $1394\,\mathrm{cm}^{-1}$, and $1436\,\mathrm{cm}^{-1}$) further confirmed the modification of graphene surface with linker molecules.

AFM was used to characterize the surface morphology of graphene surface upon individual functionalization steps. The modification of the surface by PSE molecules indistinguishable in the AFM images, but the line spectra confirmed the formation of a PSE layer with a thickness of $\sim 1\,\mathrm{nm}$ on the graphene surface. A clear modification of the surface occurred due to GOx immobilization, with the appearance of peaks having similar height and good distribution on the sample surface. The GOx coverage led to an additional average height increase of $4 - 5\,\mathrm{nm}$, such results show good agreement with expected dimensions of the GOx molecule.

Furthermore, it was successfully demonstrated that glucose can be detected using a biosensor based on functionalized graphene. The detection of glucose was performed at varying glucose concentrations in the phosphate buffered saline. The fabricated biosensor was tested in the solution gated FET setup with concentrations range of $0 - 21\,\mathrm{mM}$. When only PBS was present in the detection area, the graphene channel was n-doped with the Dirac point at the gate voltage -0.29 V. The Dirac point shifted towards positive values up to -0.20 V when glucose was introduced to the electrolyte

and caused p-doping of graphene.

The continuous response of the sensor was tested and monitored through changes in resistance of the functionalized graphene channel. The range of glucose concentration from 5 up to 40 mM was measured with different steps. In agreement with results from previously published studies [17, 19, 60], a change in concentration of 10 mM results in changes resistance corresponding to µA units in the drain-source current. Real-time measurements confirmed that the presence of glucose caused p-doping of the graphene channel, as was the case with the transfer curves. Both measured setups show that the sensor response is reversible, however, during intensive measurements a gradual delay of the sensor response and depletion of the activity of the enzyme GOx occur.

In this work, a biosensor based on the functionalization of CVD graphene was successfully designed, manufactured, and tested for glucose detection. This report should provide a springboard for the further development of graphene-based biosensors not only in our laboratories. The initial functionalization of graphene by a PSE linker allows the immobilization of several different receptor molecules utilized for the detection of biological substances. These include, for example, probe aptamers for DNA detection [52], as well as exosomes [31], cortisol [99], Escherichia coli[100], or SARS-CoV-2 spike [112] antibodies.

ACKNOWLEDGEMENT

I would like to acknowledge the support of ON Semiconductor®.

Bibliography

[1] Turner, A., I. Karube a G. Wilson. *Biosensors: Fundamentals and Applications*. Oxford University Press, 1987, Oxford science publications. ISBN 9780198547242.

[2] Ronkainen, N. J., H. B. Halsall a W. R. Heineman. Electrochemical biosensors. *Chemical Society Reviews*. 2010, 39(5. ISSN 0306-0012. doi:10.1039/b714449k.

[3] Clark, L. C. a C. Lyons. ELECTRODE SYSTEMS FOR CONTINUOUS MONITORING IN CARDIOVASCULAR SURGERY. *Annals of the New York Academy of Sciences*. 1962, 102(1), s. 29–45. ISSN 00778923. doi:10.1111/j.1749-6632.1962.tb13623.x.

[4] Cho, I.-H., D. H. Kim a S. Park. Electrochemical biosensors. *Biomaterials Research*. 2020, 24(1). ISSN 2055-7124. doi:10.1186/s40824-019-0181-y.

[5] Pohanka, M. a P. Skládal. Electrochemical biosensors - principles and applications. *Journal of Applied Biomedicine*. 2008, 6(2), s. 57–64. ISSN 1214021X. doi:10.32725/jab.2008.008.

[6] Sassolas, A., L. J. Blum a B. D. Leca-Bouvier. Immobilization strategies to develop enzymatic biosensors. *Biotechnology Advances*. 2012, 30(3), s. 489–511. ISSN 07349750. doi:10.1016/j.biotechadv.2011.09.003.

[7] Navaee, A. a A. Salimi. Enzyme-based electrochemical biosensors. In *Electrochemical Biosensors*. -: Elsevier, 2019. s. 167–211. doi:10.1016/B978-0-12-816491-4.00007-3. ISBN 9780128164914.

[8] Wang, J. Electrochemical Glucose Biosensors. *Chemical Reviews*. 2008, 108(2), s. 814–825. ISSN 0009-2665. doi:10.1021/cr068123a.

[9] Rao, A., M. Avula a D. Grainger. 3.34 Biomaterials Challenges in Continuous Glucose Monitors In Vivo. In *Comprehensive Biomaterials II*. -: Elsevier, 2017. s. 755–770. doi:10.1016/B978-0-12-803581-8.09314-0. ISBN 9780081006924.

[10] Pohanka, M. *Přehled biochemie*. 11 2015. ISBN 978-80-7231-358-7.

[11] Clark, L. C. et al. Continuous Recording of Blood Oxygen Tensions by Polarography. *Journal of Applied Physiology*. 1953, 6(3), s. 189–193. ISSN 8750-7587. doi:10.1152/jappl.1953.6.3.189.

[12] Guilbault, G. a G. Lubrano. An enzyme electrode for the amperometric determination of glucose. *Analytica Chimica Acta*. 1973, 64(3), s. 439–455. ISSN 00032670. doi:10.1016/S0003-2670(01)82476-4.

[13] Xu, L. et al. Biosensor Based on Self-Assembling Glucose Oxidase and Dendrimer-Encapsulated Pt Nanoparticles on Carbon Nanotubes for Glucose Detection. *Electroanalysis*. 2007, 19(6), s. 717–722. ISSN 10400397. doi:10.1002/elan.200603805.

[14] Bianco, P., J. Haladjian a C. Bourdillon. Immobilization of glucose oxidase on carbon electrodes. *Journal of Electroanalytical Chemistry and Interfacial Electrochemistry*. 1990, 293(1-2), s. 151–163. ISSN 00220728. doi:10.1016/0022-0728(90)80059-F.

[15] Zhu, L. A novel flow through optical fiber biosensor for glucose based on luminol electrochemiluminescence. *Sensors and Actuators B: Chemical*. 2002, 86(2-3), s. 209–214. ISSN 09254005. doi:10.1016/S0925-4005(02)00173-9.

[16] Rubianes, M. D. a G. A. Rivas. Carbon nanotubes paste electrode. *Electrochemistry Communications*. 2003, 5(8), s. 689–694. ISSN 13882481. doi:10.1016/S1388-2481(03)00168-1.

[17] You, X. a J. J. Pak. Graphene-based field effect transistor enzymatic glucose biosensor using silk protein for enzyme immobilization and device substrate. *Sensors and Actuators B: Chemical*. 2014, (202), s. 1357–1365. ISSN 09254005. doi:10.1016/j.snb.2014.04.079.

[18] BARSAN, M. et al. Design and application of a flow cell for carbon-film based electrochemical enzyme biosensors. *Talanta*. 2007, 71(5), s. 1893–1900. ISSN 00399140. doi:10.1016/j.talanta.2006.08.032.

[19] Kwak, Y. H. et al. Flexible glucose sensor using CVD-grown graphene-based field effect transistor. *Biosensors and Bioelectronics*. 2012, 37(1), s. 82–87. ISSN 09565663. doi:10.1016/j.bios.2012.04.042.

[20] Li, Z. et al. Effect of airborne contaminants on the wettability of supported graphene and graphite. *Nature Materials*. 2013, 12(10), s. 925–931. ISSN 1476-1122. doi:10.1038/nmat3709.

[21] Rafiee, J. et al. Wetting transparency of graphene. *Nature Materials*. 2012, 11(3), s. 217–222. ISSN 1476-1122. doi:10.1038/nmat3228.

[22] Novoselov, K. S. Electric Field Effect in Atomically Thin Carbon Films. *Science*. 2004, 306(5696), s. 666–669. ISSN 0036-8075. doi:10.1126/science.1102896.

[23] Molitor, F. et al. Electronic properties of graphene nanostructures. *Journal of Physics: Condensed Matter*. 2011, 23(24). ISSN 0953-8984. doi:10.1088/0953-8984/23/24/243201.

[24] Chen, X., L. Zhang a S. Chen. Large area CVD growth of graphene. *Synthetic Metals*. 2015, (210), s. 95–108. ISSN 03796779. doi:10.1016/j.synthmet.2015.07.005.

[25] Bai, H., C. Li a G. Shi. Functional Composite Materials Based on Chemically Converted Graphene. *Advanced Materials*. 2011, 23(9), s. 1089–1115. ISSN 09359648. doi:10.1002/adma.201003753.

[26] Novoselov, K. S. et al. A roadmap for graphene. *Nature*. 2012, 490(7419), s. 192–200. ISSN 0028-0836. doi:10.1038/nature11458.

[27] Novoselov, K. S. et al. Two-dimensional atomic crystals. *Proceedings of the National Academy of Sciences*. 2005, 102(30), s. 10451–10453. ISSN 0027-8424. doi:10.1073/pnas.0502848102.

[28] He, Q. et al. Graphene-based electronic sensors. *Chemical Science*. 2012, 3(6). ISSN 2041-6520. doi:10.1039/c2sc20205k.

[29] Wang, R. et al. Graphene based functional devices. *Frontiers of Physics*. 2019, 14(1). ISSN 2095-0462. doi:10.1007/s11467-018-0859-y.

[30] Haslam, C. et al. Label-Free Sensors Based on Graphene Field-Effect Transistors for the Detection of Human Chorionic Gonadotropin Cancer Risk Biomarker. *Diagnostics*. 2018, 8(1). ISSN 2075-4418. doi:10.3390/diagnostics8010005.

[31] Tsang, D. K. H. et al. Chemically Functionalised Graphene FET Biosensor for the Label-free Sensing of Exosomes. *Scientific Reports*. 2019, 9(1). ISSN 2045-2322. doi:10.1038/s41598-019-50412-9.

[32] Pumera, M. Graphene in biosensing. *Materials Today*. 2011, 14(7-8), s. 308–315. ISSN 13697021. doi:10.1016/S1369-7021(11)70160-2.

[33] Chauhan, N., T. Maekawa a D. N. S. Kumar. Graphene based biosensors—Accelerating medical diagnostics to new-dimensions. *Journal of Materials Research*. 2017, 32(15), s. 2860–2882. ISSN 0884-2914. doi:10.1557/jmr.2017.91.

[34] Marcano, D. C. et al. Improved Synthesis of Graphene Oxide. *ACS Nano*. 2010, 4(8), s. 4806–4814. ISSN 1936-0851. doi:10.1021/nn1006368.

[35] Chung, C. et al. Biomedical Applications of Graphene and Graphene Oxide. *Accounts of Chemical Research*. 2012, 46(10), s. 2211–2224. ISSN 0001-4842. doi:10.1021/ar300159f.

[36] Liu, Y. et al. Biocompatible Graphene Oxide-Based Glucose Biosensors. *Langmuir*. 2010, 26(9), s. 6158–6160. ISSN 0743-7463. doi:10.1021/la100886x.

[37] Jung, J. et al. A Graphene Oxide Based Immuno-biosensor for Pathogen Detection. *Angewandte Chemie International Edition*. 2010, 49(33), s. 5708–5711. ISSN 14337851. doi:10.1002/anie.201001428.

[38] Yu, W. et al. Progress in the functional modification of graphene/graphene oxide. *RSC Advances*. 2020, 10(26), s. 15328–15345. ISSN 2046-2069. doi:10.1039/D0RA01068E.

[39] Chua, C. K. a M. Pumera. Covalent chemistry on graphene. *Chemical Society Reviews*. 2013, 42(8). ISSN 0306-0012. doi:10.1039/c2cs35474h.

[40] Georgakilas, V. et al. Functionalization of Graphene. *Chemical Reviews*. 2012, 112(11), s. 6156–6214. ISSN 0009-2665. doi:10.1021/cr3000412.

[41] Radical (free radical). In *IUPAC Compendium of Chemical Terminology*. Research Triagle Park, NC: IUPAC, 2009. doi:10.1351/goldbook.R05066. Available from: `http://goldbook.iupac.org/R05066.html`. ISBN 0-9678550-9-8.

[42] Chapter 10: Conjugation in Alkadienes and Allylic Systems, 2006. Available from: `https://slideplayer.com/slide/8584507/`.

[43] Niyogi, S. et al. Spectroscopy of Covalently Functionalized Graphene. *Nano Letters*. 2010, 10(10), s. 4061–4066. ISSN 1530-6984. doi:10.1021/nl1021128.

[44] Jin, Z. et al. Click Chemistry on Solution-Dispersed Graphene and Monolayer CVD Graphene. *Chemistry of Materials*. 2011, 23(14), s. 3362–3370. ISSN 0897-4756. doi:10.1021/cm201131v.

[45] Liu, H. et al. Photochemical Reactivity of Graphene. *Journal of the American Chemical Society*. 2009, 131(47), s. 17099–17101. ISSN 0002-7863. doi:10.1021/ja9043906.

[46] Bao, Q. et al. Graphene-Polymer Nanofiber Membrane for Ultrafast Photonics. *Advanced Functional Materials*. 2010, 20(5), s. 782–791. ISSN 1616301X. doi:10.1002/adfm.200901658.

[47] *Organic Reactions*. John Wiley & Sons, Inc, 2004. ISBN 0471264180.

[48] Georgakilas, V. et al. Organic functionalisation of graphenes. *Chemical Communications*. 2010, 46(10). ISSN 1359-7345. doi:10.1039/b922081j.

[49] Zhang, X. et al. One-Pot Functionalization of Graphene with Porphyrin through Cycloaddition Reactions. *Chemistry - A European Journal*. 2011, 17(32), s. 8957–8964. ISSN 09476539. doi:10.1002/chem.201100980.

[50] Fang, M. et al. Covalent polymer functionalization of graphene nanosheets and mechanical properties of composites. *Journal of Materials Chemistry*. 2009, 19(38). ISSN 0959-9428. doi:10.1039/b908220d.

[51] Hunter, C. A. a J. K. M. Sanders. The nature of .pi.-.pi. interactions. *Journal of the American Chemical Society*. 1990, 112(14), s. 5525–5534. ISSN 0002-7863. doi:10.1021/ja00170a016.

[52] Yue, W. et al. An electricity-fluorescence double-checking biosensor based on graphene for detection of binding kinetics of DNA hybridization. *RSC Advances*. 2017, 7(70), s. 44559–44567. ISSN 2046-2069. doi:10.1039/C7RA08246K.

[53] Kumar, N. et al. Detection of a multi-disease biomarker in saliva with graphene field effect transistors. *Medical & sensors*. 2020, 3(6). ISSN 2573-802X. doi:10.1002/mds3.10121.

[54] Zhang, Y. et al. An optic-fiber graphene field effect transistor biosensor for the detection of single-stranded DNA. *Analytical Methods*. 2021, 13(15), s. 1839–1846. ISSN 1759-9660. doi:10.1039/D1AY00101A.

[55] Wang, X., S. M. Tabakman a H. Dai. Atomic Layer Deposition of Metal Oxides on Pristine and Functionalized Graphene. *Journal of the American Chemical Society*. 2008, 130(26), s. 8152–8153. ISSN 0002-7863. doi:10.1021/ja8023059.

[56] Wang, Q. H. a M. C. Hersam. Room-temperature molecular-resolution characterization of self-assembled organic monolayers on epitaxial graphene. *Nature Chemistry*. 2009, 1(3), s. 206–211. ISSN 1755-4330. doi:10.1038/nchem.212.

[57] Liu, J. et al. Thermosensitive graphene nanocomposites formed using pyrene-terminal polymers made by RAFT polymerization. *Journal of Polymer Science Part A: Polymer Chemistry*. 2010, 48(2), s. 425–433. ISSN 0887624X. doi:10.1002/pola.23802.

[58] Kodali, V. K. et al. Nonperturbative Chemical Modification of Graphene for Protein Micropatterning. *Langmuir*. 2011, 27(3), s. 863–865. ISSN 0743-7463. doi:10.1021/la1033178.

[59] Besteman, K. et al. Enzyme-Coated Carbon Nanotubes as Single-Molecule Biosensors. *Nano Letters*. 2003, 3(6), s. 727–730. ISSN 1530-6984. doi:10.1021/nl034139u.

[60] Huang, Y. et al. Nanoelectronic biosensors based on CVD grown graphene. *Nanoscale*. 2010, 2(8). ISSN 2040-3364. doi:10.1039/c0nr00142b.

[61] Wu, G. et al. Doping effects of surface functionalization on graphene with aromatic molecule and organic solvents. *Applied Surface Science*. 2017, (425), s. 713–721. ISSN 01694332. doi:10.1016/j.apsusc.2017.07.048.

[62] Liu, Y. et al. Giant enhancement in vertical conductivity of stacked CVD graphene sheets by self-assembled molecular layers. *Nature Communications*. 2014, 5(1). ISSN 2041-1723. doi:10.1038/ncomms6461.

[63] Georgakilas, V. et al. Noncovalent Functionalization of Graphene and Graphene Oxide for Energy Materials, Biosensing, Catalytic, and Biomedical Applications. *Chemical Reviews*. 2016, 116(9), s. 5464–5519. ISSN 0009-2665. doi:10.1021/acs.chemrev.5b00620.

[64] Guo, B. et al. Graphene Doping. *Insciences Journal*. 2011, s. 80–89. ISSN 1664171X. doi:10.5640/insc.010280.

[65] Liu, H., Y. Liu a D. Zhu. Chemical doping of graphene. *J. Mater. Chem.* 2011, 21(10), s. 3335–3345. ISSN 0959-9428. doi:10.1039/C0JM02922J.

[66] Ferrari, A. C. a D. M. Basko. Raman spectroscopy as a versatile tool for studying the properties of graphene. *Nature Nanotechnology.* 2013, 8(4), s. 235–246. ISSN 1748-3387. doi:10.1038/nnano.2013.46.

[67] *Spectroscopic methods for nanomaterials characterization. Volume 2 / edited by Sabu Thomas.* Elsevier, 2017, Micro & Nano Technologies Series. ISBN 0-323-46146-8.

[68] Pavlásková, L. *Šíření náboje studované pomocí Kelvinovy sondové mikroskopie na selektivně hydrogenovaném grafenu.* PhD thesis, Vysoké učení technické v Brně, Fakulta strojního inženýrství, 2019.

[69] Mironov, V. *Fundamentals of Scanning Probe Microscopy.* 01 2014.

[70] Béraud, A. et al. Graphene field-effect transistors as bioanalytical sensors. *The Analyst.* 2021, 146(2), s. 403–428. ISSN 0003-2654. doi:10.1039/D0AN01661F.

[71] Boušek, J., P. Kosina a B. Mojrová. *Elektronické součástky.* Vysoké učení technické v Brně, 2015.

[72] Ohno, Y. et al. Electrolyte-Gated Graphene Field-Effect Transistors for Detecting pH and Protein Adsorption. *Nano Letters.* 2009, 9(9), s. 3318–3322. ISSN 1530-6984. doi:10.1021/nl901596m.

[73] Vu a Chen. Field-Effect Transistor Biosensors for Biomedical Applications. *Sensors.* 2019, 19(19). ISSN 1424-8220. doi:10.3390/s19194214.

[74] Sadighbayan, D., M. Hasanzadeh a E. Ghafar-Zadeh. Biosensing based on field-effect transistors (FET). *TrAC Trends in Analytical Chemistry.* 2020, 133. ISSN 01659936. doi:10.1016/j.trac.2020.116067.

[75] Gelmont, B., M. Shur a R. Mattauch. Disk and stripe capacitances. *Solid-State Electronics.* 1995, 38(3), s. 731–734. ISSN 00381101. doi:10.1016/0038-1101(94)00140-B.

[76] Stassen, A. F. et al. Influence of the gate dielectric on the mobility of rubrene single-crystal field-effect transistors. *Applied Physics Letters.* 2004, 85(17), s. 3899–3901. ISSN 0003-6951. doi:10.1063/1.1812368.

[77] Kim, T. et al. Large-Scale Graphene Micropatterns via Self-Assembly-Mediated Process for Flexible Device Application. *Nano Letters.* 2012, 12(2), s. 743–748. ISSN 1530-6984. doi:10.1021/nl203691d.

[78] Gierz, I. et al. Atomic Hole Doping of Graphene. *Nano Letters.* 2008, 8(12), s. 4603–4607. ISSN 1530-6984. doi:10.1021/nl802996s.

[79] An, Y. et al. Metal-semiconductor-metal photodetectors based on graphene/ p -type silicon Schottky junctions. *Applied Physics Letters*. 2013, 102(1). ISSN 0003-6951. doi:10.1063/1.4773992.

[80] Shim, N. Y. et al. All-Plastic Electrochemical Transistor for Glucose Sensing Using a Ferrocene Mediator. *Sensors*. 2009, 9(12), s. 9896–9902. ISSN 1424-8220. doi:10.3390/s91209896.

[81] Shin, D. H. et al. Highly selective FET-type glucose sensor based on shape-controlled palladium nanoflower-decorated graphene. *Sensors and Actuators B: Chemical*. 2018, (264), s. 216–223. ISSN 09254005. doi:10.1016/j.snb.2018.02.139.

[82] Chen, R. J. et al. Noncovalent Sidewall Functionalization of Single-Walled Carbon Nanotubes for Protein Immobilization. *Journal of the American Chemical Society*. 2001, 123(16), s. 3838–3839. ISSN 0002-7863. doi:10.1021/ja010172b.

[83] Wu, G. et al. Chemical functionalization of graphene with aromatic molecule. In *2015 IEEE 15th International Conference on Nanotechnology (IEEE-NANO)*, s. 1324–1327. IEEE, 2015. doi:10.1109/NANO.2015.7388878. ISBN 978-1-4673-8156-7.

[84] Viswanathan, S. et al. Graphene–protein field effect biosensors. *Materials Today*. 2015, 18(9), s. 513–522. ISSN 13697021. doi:10.1016/j.mattod.2015.04.003.

[85] 1-Pyrenebutanoic acid succinimidyl ester. In *Handbook of Fluorescent Dyes and Probes*. Hoboken, NJ, USA: John Wiley & Sons, 2015. s. 336–339. doi:10.1002/9781119007104.ch124. ISBN 9781119007104.

[86] Prakash, R. et al. Functionalization of carbon nanotubes with proteins and quantum dots in aqueous buffer solutions. *Applied Physics Letters*. 2006, 88(6). ISSN 0003-6951. doi:10.1063/1.2171802.

[87] Han, S.-P., T. Cagin a W. A. Goddard. Understanding Noncovalent Absorption and Packing of 1-Pyrene Butanoic Acid Succinimidyl Ester on Single Walled Carbon Nanotubes. *MRS Proceedings*. 2003, 772), s. –. ISSN 0272-9172. doi:10.1557/PROC-772-M6.3.

[88] Lu, S. et al. Stabilization of Enzymes in Silk Films. *Biomacromolecules*. 2009, 10(5), s. 1032–1042. ISSN 1525-7797. doi:10.1021/bm800956n.

[89] Zhang, M. et al. Highly sensitive glucose sensors based on enzyme-modified whole-graphene solution-gated transistors. *Scientific Reports*. 2015, 5(1). ISSN 2045-2322. doi:10.1038/srep08311.

[90] Wohlfahrt, G. et al. 1.8 and 1.9 resolution structures of the Penicillium amagasakiense and Aspergillus niger glucose oxidases as a basis for modelling substrate complexes. *Acta Crystallographica Section D Biological Crystallography*. 1999, 55(5), s. 969–977. ISSN 0907-4449. doi:10.1107/S0907444999003431.

[91] Libertino, S. et al. XPS and AFM Characterization of the Enzyme Glucose Oxidase Immobilized on SiO 2 Surfaces. *Langmuir*. 2008, 24(5), s. 1965–1972. ISSN 0743-7463. doi:10.1021/la7029664.

[92] Gelardi, G. a R. Flatt. Working mechanisms of water reducers and superplasticizers. In *Science and Technology of Concrete Admixtures*. Elsevier, 2016. s. 257–278. doi:10.1016/B978-0-08-100693-1.00011-4. ISBN 9780081006931.

[93] Hu, S.-W. et al. Peculiar Wetting of N , N -Dimethylformamide. *The Journal of Physical Chemistry C*. 2019, 123(40), s. 24477–24486. ISSN 1932-7447. doi:10.1021/acs.jpcc.9b04353.

[94] Choi, J.-Y., T. L. Alford a C. B. Honsberg. Solvent-Controlled Spin-Coating Method for Large-Scale Area Deposition of Two-Dimensional Silica Nanosphere Assembled Layers. *Langmuir*. 2014, 30(20), s. 5732–5738. ISSN 0743-7463. doi:10.1021/la5001842.

[95] Ráhová, J. Využití Ramanovského mapování pro studium uhlíkaté hmoty hornin. Diplomová práce, Univerzita Karlova, Přírodovědecká fakulta, Praha, 2017.

[96] Almeida, P. R. et al. Development of a Graphene-Based Biosensor for Detecting Recombinant Cyanovirin-N. *Biosensors*. 2020, 10(12). ISSN 2079-6374. doi:10.3390/bios10120206.

[97] Casiraghi, C. et al. Raman fingerprint of charged impurities in graphene. *Applied Physics Letters*. 2007, 91(23. ISSN 0003-6951. doi:10.1063/1.2818692.

[98] Tian, M. et al. RNA Detection Based on Graphene Field-Effect Transistor Biosensor. *Advances in Condensed Matter Physics*. 2018, (2018), s. 1–6. ISSN 1687-8108. doi:10.1155/2018/8146765.

[99] Maidin, N. N. M. et al. Interaction of graphene electrolyte gate field-effect transistor for detection of cortisol biomarker. In -, s. 020022, 2018. doi:10.1063/1.5080835.

[100] Wu, G., M. Meyyappan a K. W. C. Lai. Graphene field-effect transistors-based biosensors for Escherichia coli detection. In *2016 IEEE 16th International Conference on Nanotechnology (IEEE-NANO)*, s. 22–25. IEEE, 2016. doi:10.1109/NANO.2016.7751414. ISBN 978-1-5090-1493-4.

[101] Losic, D., J. G. Shapter a J. J. Gooding. Scanning Tunneling Microscopy Studies of Glucose Oxidase on Gold Surfaces. *Langmuir*. 2002, 18(14), s. 5422–5428. ISSN 0743-7463. doi:10.1021/la015654f.

[102] Ping, J. et al. Scalable Production of High-Sensitivity, Label-Free DNA Biosensors Based on Back-Gated Graphene Field Effect Transistors. *ACS Nano*. 2016, 10(9), s. 8700–8704. ISSN 1936-0851. doi:10.1021/acsnano.6b04110.

[103] Gooding, J. J. et al. An assay for the determination of the amount of glucose oxidase immobilised in an enzyme electrode. *Analytical Communications*. 36(6), s. 225–228. ISSN 13597337. doi:10.1039/a902718a.

[104] Urbiš, J. *Optimalizace a měření transportních experimentů na grafenových polem řízených tranzistorech*. PhD thesis, Vysoké učení technické v Brně, Fakulta strojního inženýrství, 2019.

[105] Zhao, R. et al. Enhancing direct electron transfer of glucose oxidase using a gold nanoparticle |titanate nanotube nanocomposite on a biosensor. *Electrochimica Acta*. 2015, (163), s. 64–70. ISSN 00134686. doi:10.1016/j.electacta.2015.02.098. Available from: `https://linkinghub.elsevier.com/retrieve/pii/S0013468615003849`.

[106] Hwang, M. T. et al. Highly specific SNP detection using 2D graphene electronics and DNA strand displacement. *Proceedings of the National Academy of Sciences*. 2016, 113(26), s. 7088–7093. ISSN 0027-8424. doi:10.1073/pnas.1603753113.

[107] Liu, F. et al. Micropatterned reduced graphene oxide based field-effect transistor for real-time virus detection. *Sensors and Actuators B: Chemical*. 2013, (186), s. 252–257. ISSN 09254005. doi:10.1016/j.snb.2013.05.097.

[108] Lerner, M. B. et al. Scalable Production of Highly Sensitive Nanosensors Based on Graphene Functionalized with a Designed G Protein-Coupled Receptor. *Nano Letters*. 2014, 14(5), s. 2709–2714. ISSN 1530-6984. doi:10.1021/nl5006349.

[109] Jin, X. et al. A field effect transistor modified with reduced graphene oxide for immunodetection of Ebola virus. *Microchimica Acta*. 2019, 186(4). ISSN 0026-3672. doi:10.1007/s00604-019-3256-5.

[110] Seo, G. et al. Rapid Detection of COVID-19 Causative Virus (SARS-CoV-2) in Human Nasopharyngeal Swab Specimens Using Field-Effect Transistor-Based Biosensor. *ACS Nano*. 2020, 14(4), s. 5135–5142. ISSN 1936-0851. doi:10.1021/acsnano.0c02823.

[111] Zhang, X. et al. Electrical probing of COVID-19 spike protein receptor binding domain via a graphene field-effect transistor, 2020.

[112] Sengupta, J. a C. M. Hussain. Graphene-based field-effect transistor biosensors for the rapid detection and analysis of viruses. *Carbon Trends*. 2021, 2. ISSN 26670569. doi:10.1016/j.cartre.2020.100011.

8. Supplementary material

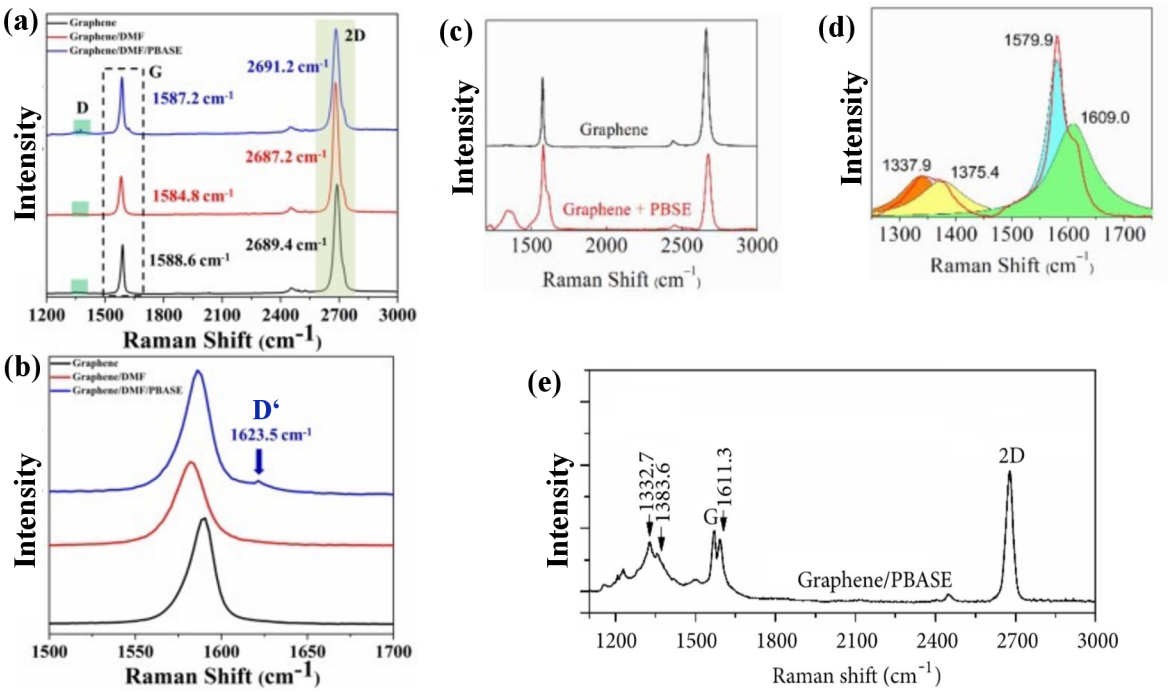

Figure 8.1: Raman spectra of graphene before and after PSE functionalization from previous studies showing characteristic features induced by PSE molecules. Ref. [61]: (a) Raman spectra before (black curve) and after (blue curve) functionalization, and (b) detailed representation of G peak with new D' peak. Green rectangle represents the disorder D peak. Ref. [96]: (c) Raman spectra before (black curve) and after (red curve) functionalization, and (d) detailed representation of the region near G band. Ref.[98]: Raman spectrum of graphene after PSE functionalization with several new bands observed near the D and G peaks.